EUROPEAN ORGANIZATION FOR NUCLEAR RESEARCH (CERN)

CERN-PH-EP/2013-133
2013/08/20

CMS-TOP-11-020

Measurement of the W-boson helicity in top-quark decays from $t\bar{t}$ production in lepton+jets events in pp collisions at $\sqrt{s} = 7\,\text{TeV}$

The CMS Collaboration*

Abstract

The W-boson helicity fractions in top-quark decays are measured with $t\bar{t}$ events in the lepton+jets final state, using proton-proton collisions at a centre-of-mass energy of 7 TeV, collected in 2011 with the CMS detector at the LHC. The data sample corresponds to an integrated luminosity of $5.0\,\text{fb}^{-1}$. The measured fractions of longitudinal, left-, and right-handed helicity are $F_0 = 0.682 \pm 0.030\,(\text{stat.}) \pm 0.033\,(\text{syst.})$, $F_L = 0.310 \pm 0.022\,(\text{stat.}) \pm 0.022\,(\text{syst.})$, and $F_R = 0.008 \pm 0.012\,(\text{stat.}) \pm 0.014\,(\text{syst.})$, consistent with the standard model predictions. The measured fractions are used to probe the existence of anomalous Wtb couplings. Exclusion limits on the real components of the anomalous couplings g_L, g_R are also derived.

Submitted to the Journal of High Energy Physics

*See Appendix A for the list of collaboration members

1 Introduction

Following the discovery of the top quark in proton-antiproton collisions at the Tevatron collider [1, 2], measurements of W-boson helicity fractions in top-quark decays have been an important subject of investigation, because of their relationship to the V−A structure of the weak charged current and their sensitivity to physics beyond the standard model (SM). With the large samples of $\mathrm{t\bar{t}}$ events produced in proton-proton collisions at the Large Hadron Collider (LHC), the W-boson helicity fraction measurements can be improved considerably, enhancing the search for anomalous Wtb couplings, i.e. those that do not arise from the SM. Previous measurements of W-boson helicity fractions in top-quark decays have been performed by the CDF, D0 [3], and ATLAS [4] Collaborations.

The helicity fractions of the W boson produced in a $\mathrm{t} \to \mathrm{Wb}$ decay are defined as the partial rate for a given helicity state divided by the total decay rate: $F_{L,R,0} \equiv \Gamma_{L,R,0}/\Gamma$, where F_L, F_R, and F_0 are the left-handed, right-handed, and longitudinal helicity fractions, respectively. For SM couplings and unpolarised top-quark production, the helicity fractions are approximately 70% longitudinal and 30% left-handed. At leading order (LO) and in the limit $m_\mathrm{b} = 0$ (where m_b is the b-quark mass), the right-handed helicity fraction is zero due to helicity suppression. For finite m_b, the helicity fractions are [5] :

$$F_0 = \frac{(1-y^2)^2 - x^2(1+y^2)}{(1-y^2)^2 + x^2(1-2x^2+y^2)}, \tag{1}$$

$$F_L = \frac{x^2(1-x^2+y^2+\sqrt{\lambda})}{(1-y^2)^2 + x^2(1-2x^2+y^2)}, \tag{2}$$

$$F_R = \frac{x^2(1-x^2+y^2-\sqrt{\lambda})}{(1-y^2)^2 + x^2(1-2x^2+y^2)}, \tag{3}$$

where $x = M_\mathrm{W}/m_\mathrm{t}$, $y = m_\mathrm{b}/m_\mathrm{t}$, $\lambda = 1 + x^4 + y^4 - 2x^2y^2 - 2x^2 - 2y^2$, and M_W, m_t are the masses of the W boson and top quark, respectively. These fractions are minimally modified by higher-order corrections. Recent next-to-next-to-leading-order (NNLO) calculations [6] predict $F_0 = 0.687 \pm 0.005$, $F_L = 0.311 \pm 0.005$, and $F_R = 0.0017 \pm 0.0001$ for a top-quark mass of $m_\mathrm{t} = 172.8 \pm 1.3\,\mathrm{GeV}/c^2$.

Experimentally, the W-boson helicity components can be extracted through the study of angular distributions of top-quark decay products in $\mathrm{t\bar{t}}$ final states. The helicity angle θ^* is defined as the angle between the W-boson momentum in the top-quark rest frame and the momentum of the down-type decay fermion in the rest frame of the W boson. The distribution of the cosine of the helicity angle has a dependence on the helicity fractions given by:

$$\frac{1}{\Gamma}\frac{\mathrm{d}\Gamma}{\mathrm{d}\cos\theta^*} = \frac{3}{8}F_L\,(1-\cos\theta^*)^2 + \frac{3}{4}F_0(\sin\theta^*)^2 + \frac{3}{8}F_R\,(1+\cos\theta^*)^2\,. \tag{4}$$

Deviations of the measured helicity fractions from the SM predictions can be interpreted in terms of anomalous Wtb couplings [7, 8], using the most general dimension-six Lagrangian:

$$\mathcal{L}_\mathrm{Wtb} = -\frac{g}{\sqrt{2}}\bar{b}\gamma^\mu(V_L P_L + V_R P_R)tW^-_\mu - \frac{g}{\sqrt{2}}\bar{b}\frac{i\sigma^{\mu\nu}q_\nu}{M_\mathrm{W}}\,(g_L P_L + g_R P_R)\,t\,W^-_\mu + \mathrm{h.c.}, \tag{5}$$

where V_L, V_R, g_L, g_R are dimensionless complex constants, $q = p_\mathrm{t} - p_\mathrm{b}$, where p_t (p_b) is the four-momentum of the top quark (b quark), P_L (P_R) are the left (right) projector operators, and h.c. denotes the Hermitian conjugate. Hermiticity conditions on the possible dimension-six

Lagrangians also impose $\mathrm{Im}(V_L) = 0$ [8]. In the SM and at tree level, $V_L = V_{\mathrm{tb}}$, where V_{tb} is the Cabibbo–Kobayashi–Maskawa matrix element $V_{\mathrm{tb}} \simeq 1$, and $V_R = g_L = g_R = 0$. The relation between helicity fractions and anomalous couplings, including dependencies on the b-quark mass, are given in Ref. [9].

We report on a study of the W-boson helicity fractions in top-quark decays using a sample of $\mathrm{t\bar{t}}$ events where one of the top quarks decays semileptonically (e.g. $\mathrm{t} \to \mathrm{W}^+\mathrm{b} \to \ell^+\nu_\ell\mathrm{b}$, where ℓ is either an electron or a muon) and the other decays hadronically (e.g. $\mathrm{t} \to \mathrm{W}^-\overline{\mathrm{b}} \to \mathrm{q\bar{q}'}\overline{\mathrm{b}}$). A kinematic fit is used to determine the best association of b jets, other jets, and lepton candidates to the top quark and antiquark decay hypotheses, interpreting the measured momentum imbalance as due to the presence of a neutrino. In this kinematic fit, top-quark and W-boson mass constraints are employed to improve the resolution of the measured jet and lepton energies, resulting in an improved reconstruction of the W-boson rest frame and the helicity angles in the weak decays of top quarks. In this article, the cosine of the helicity angles in the semileptonic and hadronic top-quark decays will be referred to as $\cos\theta^*$and $\cos^{\mathrm{had}}\theta^*$, respectively. In the leptonic branch, the down-type fermion corresponds to the charged lepton. In the hadronic branch, since the down-type quark is not experimentally identified, only the absolute value of $\cos^{\mathrm{had}}\theta^*$is used, providing information on the relative proportion between longitudinal (F_0) and total transverse ($F_L + F_R = 1 - F_0$) fractions. The resulting helicity angle distributions are fitted to measure the W-boson helicity fractions and to determine possible anomalous Wtb couplings.

2 The CMS detector

The central feature of the Compact Muon Solenoid (CMS) detector is a superconducting solenoid, 13 m in length and 6 m in diameter, which provides a uniform axial magnetic field of 3.8 T. The CMS experiment uses a right-handed coordinate system, with the origin at the nominal interaction point, the x axis pointing to the centre of the LHC, the y axis pointing up (perpendicular to the LHC plane), and the z axis along the anticlockwise-beam direction. The polar angle θ is measured from the positive z axis and the azimuthal angle ϕ is measured in the x-y plane. The bore of the solenoid is instrumented with various particle detection systems. Charged-particle trajectories are measured with a silicon pixel tracker with three barrel layers at radii between 4.4 and 10.2 cm, and a silicon strip tracker with 10 barrel detection layers that extend outward reaching a radius of 1.1 m. Each system is completed by two endcaps, and provides angular coverage of $0 < \phi < 2\pi$ in azimuth and $|\eta| < 2.5$, where the pseudorapidity η is defined as $\eta = -\ln[\tan(\theta/2)]$, with θ the polar angle of the trajectory of the particle with respect to the z axis. A lead-tungstate crystal electromagnetic calorimeter (ECAL) and a brass/scintillator hadron calorimeter (HCAL) surround the tracking volume and cover the region $|\eta| < 3$. The forward calorimeter further extends the HCAL coverage in the region $3 < |\eta| < 5$, improving the determination of the momentum imbalance.

Muons are measured and identified in gas-ionisation detectors embedded in the steel flux return yoke outside the solenoid in the range $|\eta| < 2.4$. The barrel region is covered by drift-tube chambers and the endcap region by cathode strip chambers, each complemented by resistive plate chambers. The detector is nearly hermetic, allowing for energy balance measurements in the plane transverse to the beam. A two-level trigger system selects the most interesting pp collision events for use in physics analysis, The first level of the CMS trigger system, composed of custom hardware processors, uses information from the calorimeters and muon detectors to select the most interesting events in a fixed time interval of less than about 3.2 μs. The second level, known as the high-level trigger (HLT), is a processor farm that further decreases the event

rate from around 100 kHz to around 300 Hz, before data storage. A more detailed description of the CMS detector can be found elsewhere [10].

3 Data and simulated samples

The measurements presented in this paper are performed using events from proton-proton collisions at a centre-of-mass energy of 7 TeV, collected by the CMS detector in 2011. The data correspond to an integrated luminosity of $5.0 \pm 0.1\,\text{fb}^{-1}$ [11]. In order to account for effects of detector resolution and acceptance, as well as to estimate the contribution from background processes that can satisfy the $\mathrm{t\bar{t}}$ event selection criteria, simulated event samples based on Monte Carlo (MC) event generator programs are used.

A $\mathrm{t\bar{t}}$ signal sample was generated using the MADGRAPH generator version 5.1.1 [12] with matrix elements having up to three extra partons in the final state and an assumed top-quark mass of $172.5\,\text{GeV}/c^2$. MADGRAPH is interfaced with PYTHIA generator version 6.424 [13] to simulate hadronization and parton fragmentation and with TAUOLA program version 27.121.5 [14] to simulate τ-lepton decays. The helicity fractions used as a SM reference are the LO predictions for $m_{\mathrm{t}} = 172.5\,\text{GeV}/c^2$: $F_0 = 0.6902$, $F_L = 0.3089$, $F_R = 0.0009$, consistent with next-to-leading-order (NLO) and NNLO expectations [5, 6].

Single-top quark events in t and tW (or W-boson associated) channels were generated using POWHEG program version 1.0 [15] and PYTHIA interfaced with TAUOLA. Other relevant background processes, such as W boson and Drell–Yan production accompanied by multiple jets, were simulated using MADGRAPH. In all LO simulations, the parton distribution function (PDF) set CTEQ6L1 [16] is used. The POWHEG simulations use the NLO set CT10 [17].

The effect of multiple proton-proton collisions occurring within the same bunch crossing (pileup events) is taken into account in the simulation and matches the pileup distribution observed in data.

4 Event reconstruction and selection

A set of requirements is applied to all samples, selecting candidate events compatible with the topology of $\mathrm{t\bar{t}}$ production. Almost all top quarks decay into a W boson and a b quark. In the decay modes considered for this study, one of the W bosons decays hadronically into two jets and the other W boson decays leptonically into an electron or muon and a neutrino. Hence, final states containing a muon or electron and at least four jets are selected for further consideration.

Top-quark decay products are reconstructed using the particle-flow (PF) algorithm described in detail in Refs. [18] and [19]. The particle-flow event reconstruction identifies and measures the properties of each particle, using an optimised combination of the information from all subdetectors. The energy of photons is directly obtained from the ECAL measurement, corrected for zero-suppression effects. The energy of electrons is determined from a combination of the momentum of the track originated at the main interaction vertex, the corresponding ECAL cluster energy, and the energy sum of all bremsstrahlung photons attached to the track. The energy of muons is obtained from the corresponding track momentum. The energy of charged hadrons is determined from a combination of the track momentum and the corresponding ECAL and HCAL energy, corrected for zero-suppression effects, and calibrated for the nonlinear response of the calorimeters. Finally, the energy of neutral hadrons is obtained from the corresponding calibrated ECAL and HCAL energy. The missing transverse energy $E_{\mathrm{T}}^{\mathrm{miss}}$ is defined as the mag-

nitude of the transverse momentum imbalance, $\vec{p}_{\mathrm{T}}^{\,\mathrm{miss}}$, which is the negative of the vectorial sum of the transverse momenta p_{T} of all the particles reconstructed with the particle-flow algorithm. Tracks belonging to the primary or secondary vertices of the most energetic pp interaction are retained, while particles identified as coming from pileup interactions are removed from the event.

Events in the muon+jets channel were selected by a trigger that required at least one isolated, high-momentum muon with a HLT p_{T} threshold varying between 17 and 24 GeV/c for the running period used in this analysis. Events containing a muon, well measured in the silicon tracker and identified in the muon chambers with $p_{\mathrm{t}} > 25\,\mathrm{GeV}/c$ and pseudorapidity $|\eta| < 2.1$, are then selected offline. The track associated with the muon candidate is required to have a minimum number of hits in the silicon tracker, to be consistent with originating from the beam spot, and to have a high-quality global fit including a minimum number of hits in the muon detector. More details on the muon quality requirements are given in [20].

The trigger used to collect events in the electron+jets channel required at least one isolated electron with $p_{\mathrm{t}} > 25\,\mathrm{GeV}/c$, accompanied by at least three jets with $p_{\mathrm{t}} > 30\,\mathrm{GeV}/c$. Electron candidates are reconstructed from clusters of energy deposits in the electromagnetic calorimeter, which are then matched to hits in the silicon tracker [21]. Electrons are identified by using shower shape and track-cluster matching variables. Offline, events with exactly one electron candidate with $p_{\mathrm{t}} > 30\,\mathrm{GeV}/c$ and $|\eta| < 2.5$ are selected. Events having electron candidates in the transition region between the barrel and endcap calorimeters, $1.44 < |\eta| < 1.56$, are excluded because reconstruction in this region is degraded due to additional material there. The electron track must lie within 0.02 cm of the primary vertex in the plane transverse to the beam axis. Additionally, the background due to electrons from photon conversions is reduced by rejecting tracks with missing hits in the inner tracker layers or that are near a track with an opposite charge and a similar polar angle.

Events with an additional muon with $p_{\mathrm{t}} > 10\,\mathrm{GeV}/c$ or and additional electron with $p_{\mathrm{t}} > 15\,\mathrm{GeV}/c$ are vetoed in order to reject backgrounds from dileptonic $\mathrm{t\bar{t}}$ and Drell–Yan events.

To reduce backgrounds further, muons and electrons are required to be prompt and are therefore typically well isolated from the rest of the event. This is achieved via an offline particle-flow-based relative isolation (PFIso) algorithm, which is defined as the sum of the transverse momenta over all charged hadrons, neutral hadrons, and photons reconstructed inside a cone of radius $\Delta R = \sqrt{(\Delta\eta)^2 + (\Delta\phi)^2} = 0.3$, centered around the lepton (muon or electron) and divided by the lepton transverse momentum. In top-quark decays, where the b jet coincidentally overlaps with the prompt lepton, $\cos\theta^*$ takes values close to -1. The offline lepton isolation requirement therefore has the effect of reducing the signal selection efficiency near $\cos\theta^* \approx -1$. In addition, both the muon and electron online triggers impose loose isolation criteria. Hence, selected muons (electrons) are required to have PFIso $< 0.125\,(0.100)$. These values are chosen to be tight enough to provide a high trigger efficiency, yet loose enough to maintain reasonable signal efficiency near $\cos\theta^* \approx -1$. In order to mitigate effects of pileup, a correction based on the average energy density in the event is applied to the electron isolation.

Jets are reconstructed using the anti-k_{T} clustering algorithm [22, 23], with a distance parameter of 0.5, applied to the entire list of reconstructed particles that are not identified as isolated muons or electrons in the event. The resulting uncalibrated jet momenta are found to be within 5% to 10% of the true momenta over the whole p_{T} spectrum and detector acceptance. Charged particles not associated with the primary vertex are explicitly removed from the jet, as stated above. A residual correction is applied to account for the energy of any extra neutral particles arising from pileup interactions. Further residual jet energy calibrations are derived from

simulation and corrected for any discrepancies with data using *in situ* measurements of object balancing in both dijet events (to render the jet response in pseudorapidity uniform) as well as photon+jet events (to provide the absolute jet energy scale) [24]. Additional selection criteria are applied to remove spurious events with identified noise patterns in the HCAL. Calibrated jets with $p_t > 10\,\text{GeV}/c$ are used to correct the scale of E_t^{miss} [25]. Jet candidates from the top-quark decay are required to have calibrated $p_t > 30\,\text{GeV}/c$ and $|\eta| < 2.4$. Events with less than four jets passing the above mentioned top-quark decay product criteria are not used in the analysis.

To reduce the QCD multijet background, the transverse mass, M_T, of the leptonically decaying W boson, is required to be greater than $30\,\text{GeV}/c^2$, where $M_T = \sqrt{2p_t E_T^{\text{miss}}(1-\cos(\Delta\phi))\times 1/c^3}$ and $\Delta\phi$ is the angle in the x-y plane between the direction of the lepton and $\vec{p}_T^{\,\text{miss}}$. In events where the top-quark pair decays dileptonically and one lepton escapes detection, the M_T variable can assume very high values. Background events from this process are rejected by requiring $M_T < 200\,\text{GeV}/c^2$.

Due to its relatively high rate and similar final state topology, the main remaining background source for this analysis is the production of several jets in association with a W boson that decays leptonically. This background source can be reduced, and the QCD multijet background even further suppressed, by requiring that at least two of the selected jets be identified as b jets. A high-efficiency tagging algorithm, known as the combined secondary-vertex (CSV) algorithm [26], is used to separate jets originating from light quarks (or gluons) and heavy quarks, i.e. charm or bottom quarks. Jets are first divided into categories according to the probability of reconstructing a secondary vertex and its quality. Then, within each category, several variables including the three-dimensional signed impact parameter significance, secondary vertex mass, fractional charge, and charged particle multiplicity are used to form a likelihood that discriminates light-flavour jets from heavy-flavour jets. A selection working point is chosen so that the efficiency to identify a b jet is high (nearly 70%), while the probability that a light-flavour jet is mistaken as a b jet is small (about 1%). Requiring that there be two b-tagged jets in the event reduces the remaining QCD multijet background to negligible levels (less than 0.4%).

Trigger, lepton identification, and lepton isolation efficiencies are estimated with a *tag-and-probe* method [27] using leptons from a sample of events containing $Z \to \ell^+\ell^-$ decays. The efficiencies are computed for the Z-boson events both data and simulation, as a function of the lepton p_T and η. The overall efficiencies in the typical p_T and η ranges of the selected leptons are 80% for muons and 70% for electrons. The ratio of the efficiencies in data and simulation, $\epsilon_\ell^{\text{DATA}}/\epsilon_\ell^{\text{MC}}$, is used as a scale factor to correct the simulated samples. Likewise, simulated samples are scaled to account for any differences in b-tagging efficiencies between data and simulation according to the ratio of efficiencies $\epsilon_{\text{b-tag}}^{\text{DATA}}/\epsilon_{\text{b-tag}}^{\text{MC}}$, which is determined as a function of the p_T of the b jet [26].

The number of data events reconstructed with these selection criteria is 9268 in the muon channel and 6526 in the electron channel. Comparisons between data observations and the SM expectations are presented in Section 8.

5 Top-quark reconstruction

Once events are selected according to the criteria described in Section 4, the reconstruction of each top-quark candidate proceeds by testing all selected jets, $\vec{p}_T^{\,\text{miss}}$, and the lepton for their compatibility with decay products of the hadronic branch ($t \to bW \to b\bar{b}'$) and the leptonic branch ($t \to bW \to b\ell\nu$). The initial value for the neutrino momentum is set to $\vec{p}^{\,\nu} = (\vec{p}_T^{\,\text{miss}}, p_z^\nu)$,

where p_z^ν is determined by requiring that the invariant mass of the neutrino and lepton be equal to the W-boson mass, which is assumed to be 80.4 GeV/c^2 [28]. For each possible neutrino solution and jet assignment to either the leptonic branch or hadronic branch, a χ^2 is built, containing the following terms:

$$\chi^2_{\text{comb}} = \left(\frac{m_{\text{t}} - m_{\text{t}}^{\text{ref}}}{\sigma_{m_{\text{t}}}}\right)^2 + \left(\frac{m_{\bar{\text{t}}} - m_{\text{t}}^{\text{ref}}}{\sigma_{m_{\bar{\text{t}}}}}\right)^2 + \left(\frac{M_{\text{W}}^{\text{lep}} - 80.4}{\sigma_{M_{\text{W}}^{\text{lep}}}}\right)^2 + \left(\frac{M_{\text{W}}^{\text{had}} - 80.4}{\sigma_{M_{\text{W}}^{\text{had}}}}\right)^2 - \sum_{i=1,4} 2 \ln p_i(\text{disc}|f), \tag{6}$$

where m_{t}, $m_{\bar{\text{t}}}$, $M_{\text{W}}^{\text{lep}}$ and $M_{\text{W}}^{\text{had}}$ are the reconstructed invariant masses for a given combinatorial assignment of four jets to the final-state particles in the $\text{t}\bar{\text{t}}$ decay. The reference value for the top-quark mass $m_{\text{t}}^{\text{ref}}$ is taken to be 173.3 GeV/c^2 [29] for data and 172.5 GeV/c^2 for the simulated samples. The term $p_i(\text{disc}|f)$ is the probability for the ith jet to have flavour f (either a b jet from the direct top-quark decay or a jet from the hadronically decaying W boson), given its measured value from the CSV tagger discriminant (see Section 4). Since the top-quark and W-boson reconstructed masses are dominated by experimental resolution effects, the parameters $\sigma_{m_{\text{t},\bar{\text{t}}}}$ and $\sigma_{M_{\text{W}}^{\text{lep, had}}}$ in Eq. (6) are approximated as Gaussian widths, which are determined from simulation.

In the process, a constrained kinematic fit is performed, which leads to an improved determination of the unmeasured neutrino momentum component p_z^ν, or in some cases a valid physical solution to be found when the analytical solution is imaginary due to detector mismeasurements, and to a more accurate reconstruction of the $\text{t}\bar{\text{t}}$ system. The momenta of the measured jets and lepton are allowed to vary within their resolutions and are required to comply with the same kinematic constraints used in Eq. (6). The t and $\bar{\text{t}}$ candidates that are chosen for further analysis correspond to the particular configuration of lepton, neutrino, and jets that minimise χ^2_{comb}. Any additional jets passing the event selection criteria that are not chosen as one of the four jets belonging to the $\text{t}\bar{\text{t}}$ system are discarded and no longer used in the analysis. Events for which the kinematic fit fails to find a real solution complying with the constraints are discarded.

Following the full event selection in simulation studies, including the requirement of at least two identified b jets, this top-quark reconstruction algorithm associates the correct jet to the leptonic top-quark decay branch in 71% of all cases. If instead one loosens the requirement to at least one b jet in the event, the fraction of correctly assigned jets to the leptonic branch decreases to 63%.

6 Background estimation

The main source of backgrounds in the analysis comes from top-quark pairs that decay into either fully leptonic or fully hadronic modes, or into semileptonic $\text{t}\bar{\text{t}}$ decays involving taus, and that pass the ℓ+jets selections. Other backgrounds are, in order of decreasing importance: single top-quark events, events from processes involving W-boson production with jets (W+jets) and Drell–Yan production with jets (DY+jets). The normalisation of the $\text{t}\bar{\text{t}}$ processes is determined by the fitting procedure described in Section 7, and the predictions for single top-quark processes are determined from simulation (see Section 3).

The cross section for inclusive W+jets and DY+jets production could be poorly predicted in the specific phase space region where those events become background for top-quark production, corresponding to high jet multiplicities and events containing heavy-flavour jets. For this

reason, the normalisation of the background coming from W+jets and DY+jets is determined using an approach partially based on the data. Muons and electrons are treated separately, since important requirements on background rejection, such as lepton isolation, are different.

6.1 Normalisation and shape of DY production with jets

The normalisation and shape of distributions from DY+jets production, are studied using a data control sample defined by applying the same selection criteria described in Section 4, except that events are required to contain an additional lepton of the same flavour and opposite charge. In this case, the M_{T} variable is computed with the event $E_{\mathrm{t}}^{\mathrm{miss}}$ and the highest-p_{T} lepton. Using a reference cross section of 3048 pb [30] for the DY production decaying into pairs of muons, electrons, and taus with invariant mass above 50 GeV/c^2, the normalisation of simulated samples for DY+jets is found to agree with the data to within the statistical uncertainty of about 10%. The following systematic uncertainties are then considered in the estimation of the normalisation scale factor $N_{\mathrm{data}}/N_{\mathrm{simulation}}$, between the amount of data and simulated events:

- the PDFs [31, 32] used to generate the samples: $\pm$3.6%;
- the uncertainties in the jet energy scale: $\pm$12.7%;
- the uncertainties in the jet energy resolution: $\pm$2.6%;
- the uncertainty in the integrated luminosity [11]: $\pm$2.2%;
- the difference observed on $N_{\mathrm{data}}/N_{\mathrm{simulation}}$ for events inside and outside a window of 30$\pm$20 GeV/c^2 around the Z-boson mass, where the DY+jets background is probed: $\pm$20.0%.

Including all systematic sources, this leads to a total estimated uncertainty of 30.0% for the DY+jets normalisation.

The shape of the $\cos\theta^*$ distribution from DY+jets background events is verified using this same control sample. The top-quark reconstruction algorithm described in Section 5 is applied, except that the highest-p_{T} lepton is used in the kinematic fit. The shapes observed in data and simulation are found to be in agreement.

6.2 Normalisation and shape of W-boson production with jets

Due to the charge of the valence quarks in the colliding protons, more positively (ℓ^+) than negatively (ℓ^-) charged leptons are produced in pp collisions for single top-quark production and W+jets events. On the other hand, the amount of ℓ^+ and ℓ^- produced in DY+jets and $\mathrm{t\bar{t}}$ processes is, to a very good approximation, the same in pp collisions. Hence, by keeping the predicted cross section of single-top-quark production fixed, the background contribution from W+jets production can be determined from the charge asymmetry $N_+ - N_-$, where N_+ (N_-) is the number of ℓ^+ (ℓ^-). The total number of W+jets events in the data sample is thus predicted to be

$$(N_+ + N_-)^{\mathrm{W+jets}}_{\mathrm{predicted}} = R^{\mathrm{W}}_{\pm(\mathrm{MC})} \times (N_+ - N_-)_{\mathrm{data}}, \tag{7}$$

where $R^{\mathrm{W}}_{\pm(\mathrm{MC})} = (N_+ + N_-)^{\mathrm{W+jets}}_{\mathrm{MC}} / (N_+ - N_-)^{\mathrm{W+jets}}_{\mathrm{MC}}$ is estimated using simulated events and $(N_+ - N_-)_{\mathrm{data}}$ is the measured asymmetry in data. The fixed contribution of single-top quark from simulation is subtracted from the total charge asymmetry in Eq. (7) so that $(N_+ - N_-)_{\mathrm{data}} = (N_+ - N_-)^{\mathrm{total}}_{\mathrm{data}} - (N_+ - N_-)^{\mathrm{single\text{-}top}}_{\mathrm{MC}}$.

The predicted normalisation is found to be consistent with the expectations from the simulation within relatively large statistical uncertainties. A total systematic uncertainty of 100% is

assigned to the normalisation of the predicted W+jets background. To test the effect of possible biases due to the assumed background shape from simulation, the analysis is repeated by dividing the data sample in bins of $\cos\theta^*$. To increase the statistical power of the test, the jet selection criteria are partially relaxed. Within the precision of the test, the shape of the $\cos\theta^*$ distribution predicted from the simulation is found to be in agreement with the data, and any possible bias is negligible compared with the normalisation uncertainty considered.

7 Determination of helicity fractions

A fitting procedure based on a MC simulation reweighting technique is used to simultaneously account for experimental resolution effects and for the dependencies on the W-boson helicity fractions. Any new helicity configuration can be obtained from the original configuration used in the simulation via an algorithm that (re)weights each event according to the generated, matrix-element level $\cos\theta^*$ values for each $W \to \ell\nu$ and $W \to q\bar{q}$ decay in the $t\bar{t}$ simulated sample.

Because of the QCD production mechanism for $t\bar{t}$ events, top quarks can be considered as unpolarised on average, to a high degree of precision. Spin correlations between the two top quarks in the event do not modify this picture. This is because the average spin properties of the top quark associated with the leptonic W-boson decay branch do not change after averaging over the phase space variables of the other top quark (from the hadronic W-boson decay branch) in the event. This scenario, which has been assumed in past and recent W-boson helicity studies [4, 33, 34], implies that the phase space density for the reconstructed $\cos\theta^*$ variable of each decay branch, $\rho(\cos\theta^*_{\text{rec}})$, can be decoupled from the rest of the event. Therefore, at matrix-element (generator) level, we assume the following dependence:

$$\rho(\cos\theta^*_{\text{gen}}) \equiv \frac{1}{N}\frac{\mathrm{d}N}{\mathrm{d}\cos\theta^*_{\text{gen}}} = \frac{3}{8}F_L(1-\cos\theta^*_{\text{gen}})^2 + \frac{3}{4}F_0\sin^2\theta^*_{\text{gen}} + \frac{3}{8}F_R(1+\cos\theta^*_{\text{gen}})^2, \qquad (8)$$

where $(F_L, F_0, F_R) \equiv \vec{F}$ are the helicity fractions to be measured, and θ^*_{gen} is the matrix-element level quantity for the helicity angle. For normalisation reasons, the helicity fractions are constrained to satisfy $F_L + F_0 + F_R = 1$. A new $\cos\theta^*_{\text{rec}}$ distribution for a particular configuration of helicity fractions F_L, F_0, F_R is then obtained by reweighting each fully simulated event by the weight

$$W(\cos\theta^*_{\text{gen}};\vec{F}) = W_{\text{lep}}(\cos\theta^*_{\text{gen}};\vec{F}) \times W_{\text{had}}(\cos\theta^*_{\text{gen}};\vec{F}), \qquad (9)$$

where $W_{\text{lep, had}}$ is defined for the leptonic and hadronic branches respectively as:

$$\begin{aligned} W_{\text{lep, had}}(\cos\theta^*_{\text{gen}};\vec{F}) &\equiv \frac{\rho(\cos\theta^*_{\text{gen}})}{\rho^{\text{SM}}(\cos\theta^*_{\text{gen}})} = \\ &= \frac{\frac{3}{8}F_L(1-\cos\theta^*_{\text{gen}})^2 + \frac{3}{4}F_0\sin^2\theta^*_{\text{gen}} + \frac{3}{8}F_R(1+\cos\theta^*_{\text{gen}})^2}{\frac{3}{8}F_L^{\text{SM}}(1-\cos\theta^*_{\text{gen}})^2 + \frac{3}{4}F_0^{\text{SM}}\sin^2\theta^*_{\text{gen}} + \frac{3}{8}F_R^{\text{SM}}(1+\cos\theta^*_{\text{gen}})^2}. \end{aligned} \qquad (10)$$

In the expression above, $F_L^{\text{SM}}, F_0^{\text{SM}}, F_R^{\text{SM}}$ are the helicity fractions that correspond to the expected SM values and which are used to generate the reference simulated sample. The new reweighted distribution automatically takes into account, by construction, all detector resolution and acceptance effects, as described by the simulation.

The helicity fractions are measured by maximising a binned Poisson likelihood function,

$$\mathcal{L}(\vec{F}) = \prod_{\text{bin } i} \frac{N_{\text{MC}}(i;\vec{F})^{N_{\text{data}}}(i)}{(N_{\text{data}}(i))!} \exp\left(-N_{\text{MC}}(i;\vec{F})\right), \tag{11}$$

which is constructed using the numbers of observed $N_{\text{data}}(i)$ and expected $N_{\text{MC}}(i;\vec{F})$ events in each $\cos\theta^*_{\text{rec}}$ bin i. The numbers of expected events are given by:

$$N_{\text{MC}}(i,\vec{F}) = N_{\text{BKG}}(i) + N_{\text{t}\bar{\text{t}}}(i;\vec{F}), \tag{12}$$

$$N_{\text{t}\bar{\text{t}}}(i;\vec{F}) = \mathcal{F}_{\text{t}\bar{\text{t}}}\left[\sum_{\text{t}\bar{\text{t}}\text{ events}} W(\cos\theta^*_{\text{gen}}(i);\vec{F})\right], \tag{13}$$

$$N_{\text{BKG}}(i) = N_{\text{W+jets}}(i) + N_{\text{DY+jets}}(i) + N_{\text{single-top}}(i) + \mathcal{F}_{\text{t}\bar{\text{t}}} \times N_{\text{t}\bar{\text{t}}\text{ non-}\ell\text{+jets}}(i). \tag{14}$$

The normalisation parameter for the $\text{t}\bar{\text{t}}$ component $\mathcal{F}_{\text{t}\bar{\text{t}}}$ is not sensitive to the helicity fractions, but it does absorb a large fraction of the experimental and theoretical systematic uncertainties in the predicted rates. Uncertainties on the normalisation of backgrounds are considered as a separate source of systematics.

Two types of fits are performed. In the fits denoted by 3D, the fractions F_0, F_L, and the normalisation factor $\mathcal{F}_{\text{t}\bar{\text{t}}}$ (see Eq. (13)) are treated as free parameters, and F_R is determined by the constraint $F_R = 1 - F_0 - F_L$. In the fits denoted by 2D, F_0 and $\mathcal{F}_{\text{t}\bar{\text{t}}}$ are taken as free parameters, setting $F_R = 0$, and solving for F_L from the constraint $F_L = 1 - F_0$. Within the expected experimental uncertainties, the $F_R = 0$ condition is satisfied both in the SM and in anomalous coupling scenarios where only g_R is different from zero.

We perform the measurements by fitting either the $\cos\theta^*$distribution from the leptonic branch or the $|\cos^{\text{had}}\theta^*|$ distribution from the hadronic branch. The two variables are fitted separately and not simultaneously, so as to avoid any possible biases due to top-quark spin correlations. At matrix-element level, $|\cos^{\text{had}}\theta^*|$ is only sensitive to the F_0 fraction (or, alternatively, to the combination $F_L + F_R$), and is therefore only used in the context of the 2D fits.

8 Comparison between data and SM predictions

The agreement between data and expectation from the SM is extensively investigated. First, the normalisations of simulated samples involving W+jets and DY+jets are determined and applied using control data samples discussed in Section 6. Next, reference cross sections 64.6 pb [35] for single-top-quark (t-channel), and 15.74 pb [36] for W-boson-associated single-top-quark processes, which correspond to approximated NNLO predictions, and NLO $\text{t}\bar{\text{t}}$ cross sections are used to scale the respective simulated samples to an integrated luminosity of $5.0\,\text{fb}^{-1}$. Finally, the simulated samples involving top quarks are corrected for both the presence of pileup and the efficiency correction factors $\epsilon_\ell^{\text{DATA}}/\epsilon_\ell^{\text{MC}}$ and $\epsilon_{\text{b-tag}}^{\text{DATA}}/\epsilon_{\text{b-tag}}^{\text{MC}}$.

Table 1 presents the number of data events observed in the muon+jets and electron+jets channels which is compared to the predictions for the signal ($\text{t}\bar{\text{t}}$) and background processes. In the table, columns two and four display the number of remaining events after applying the selection criteria described in Section 4. Columns three and five display the subsample of these events where a $\text{t}\bar{\text{t}}$ pair candidate is found, reconstructed as described in the previous section. The yields observed in data are in agreement with the predicted yields expected from the SM.

A comparison of shapes between data and simulation, after having applied the kinematic fit, for the variables relevant to this analysis is presented in figures 1 to 3. Figure 1 shows the

Table 1: Number of events expected from signal and background processes, together with the observed number of events in data for both the muon+jets and electron+jets channels. The columns labelled as "Selected" represent the number of events passing the analysis selection criteria; the columns labelled as "KF" represent the fraction of those events containing a reconstructed top-quark pair via a kinematic fit that has converged.

	muon+jets		electron+jets	
Process	Selected	KF	Selected	KF
Single top	372	319	265	223
W+jets	351	282	234	203
DY+jets	43	38	43	34
$t\bar{t}$ non ℓ+jets	928	828	629	547
Total bkg.	1694	1467	1171	1007
$t\bar{t}$ signal	7597	7321	5391	5179
Total expected	9291	8788	6562	6186
Data	9268	8772	6526	6135

kinematic distributions for the leptons in the event: transverse momentum and pseudorapidity of muons and electrons, and the neutrino transverse momentum. Figure 2 displays the p_{T} distributions for jets related to the top-quark reconstruction, including the b jets (from leptonic and hadronic tops) and the jets from the hadronic W-boson decay. The shapes of all important kinematic distributions in the data, which describe the $t\bar{t}$ system, are well reproduced by the simulation, including those that do not depend strongly on the W-boson helicity (i.e. global properties of top-quark and W-boson systems).

The most relevant distributions for this analysis, the cosine distributions of the helicity angles computed according to the definitions discussed in Section 1, are shown in figure 3 for both the muon+jets and electron+jets channels. The agreement between data and simulation for $\cos\theta^*$ and $|\cos^{\mathrm{had}}\theta^*|$ is observed to be satisfactory. This suggests that, even before any attempt to measure the W-boson helicity fractions is made, the data prefer values close to the SM predictions.

9 Systematic uncertainties

Several sources of systematic effects, which could possibly bias the measurement of the W-boson helicity fractions, have been investigated and their corresponding uncertainties in the measurement determined.

The scale of the jet energy (JES) calibration is determined from data, which is then applied as a p_{T}- and η-dependent correction to the simulation; the JES calibration has an uncertainty that typically varies between 2% and 4% [24]. To estimate the effect that the JES uncertainty has on the W-boson helicity measurement, the p_{T} of all jets are systematically shifted together, either up or down, by their corresponding p_{T}- and η-dependent uncertainty. Because the missing transverse energy is corrected due to the presence of JES calibrated jets, the systematic shifts of the jet p_{T}'s in the event are propagated and lead to systematic shifts in the momentum imbalance. The full analysis, including the reconstruction of top quarks and the resulting measurements of the W-boson helicity fractions, is then repeated. The jet energy resolution (JER) is observed to be different in data compared with the simulation. Jet energy resolutions are typically 5–13% larger in data than in simulation, with uncertainties smaller than 5% [24]. The systematic uncertainties related to JER are estimated by over-smearing the reconstructed jets

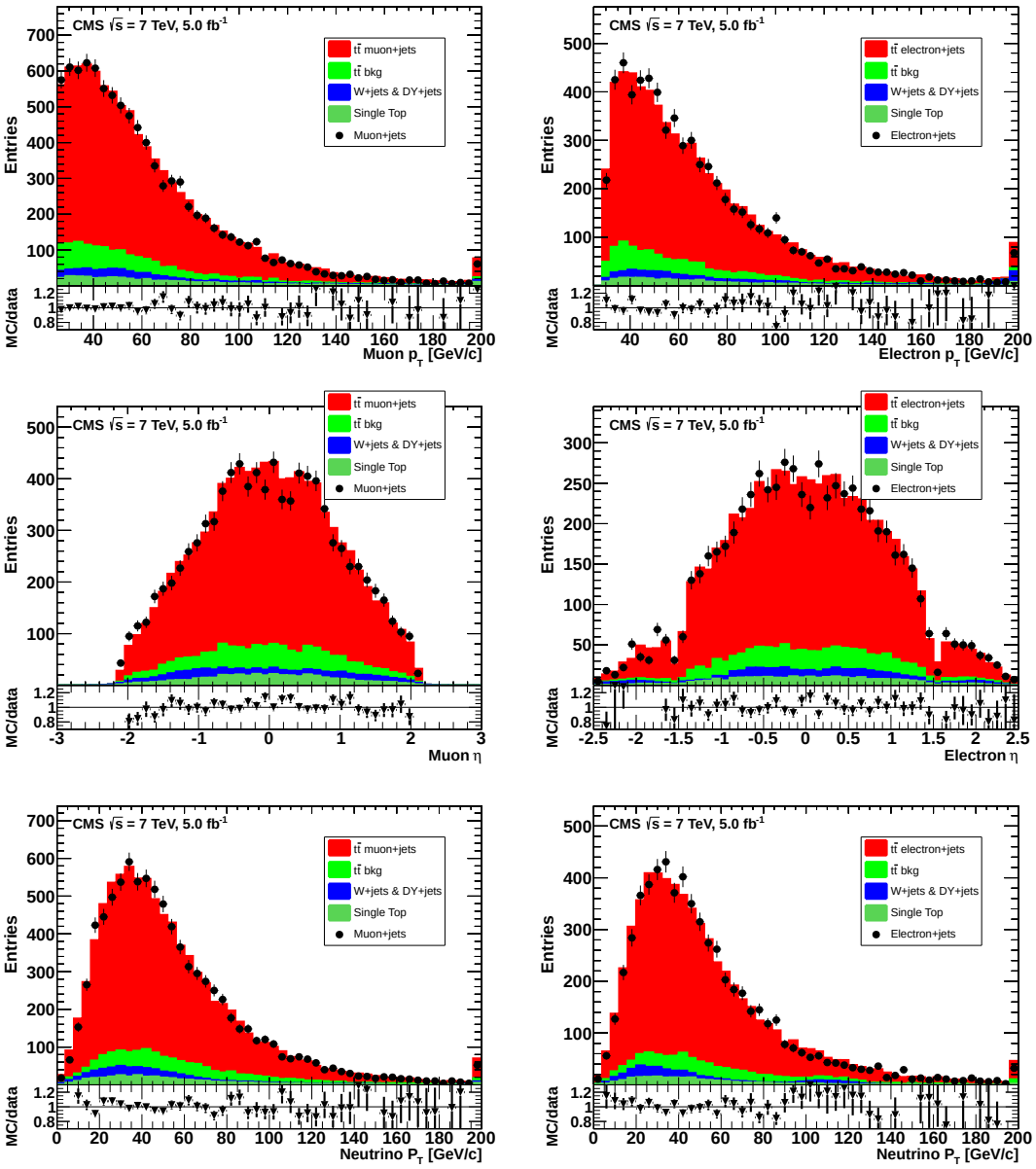

Figure 1: Distributions of data compared to SM predictions for signal and expected backgrounds: charged lepton p_{T} (top), η (centre) and neutrino p_{T} (bottom) for the muon+jets (left) and electron+jets (right) channels. Data are displayed as solid points, simulated $\mathrm{t\bar{t}}$ signal distributions as red histograms, and the contribution from other background processes as coloured histograms. Overflows are displayed in the last bin of each histogram. At the bottom, the ratio between prediction and data is displayed. Only statistical uncertainties are shown.

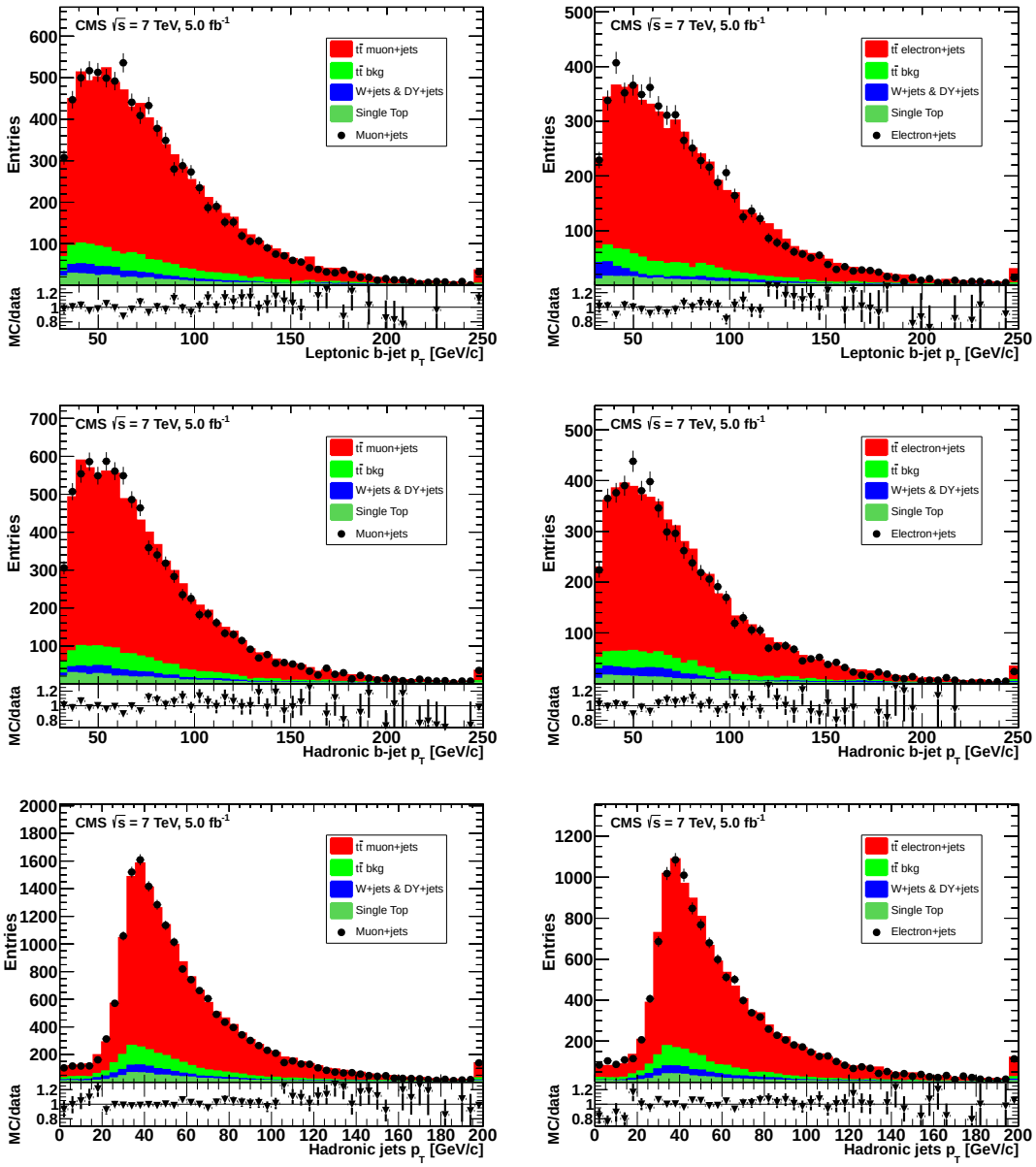

Figure 2: Distributions of transverse momenta in data compared to SM predictions for signal and expected backgrounds: the b jets identified in the leptonic (top row) and hadronic (second row) branches, and the jets from the hadronic W decay with two entries per event (bottom row) for the muon+jets (left) and electron+jets (right) channels. Data are displayed as solid points, simulated $\mathrm{t\bar{t}}$ signal distributions as red histograms, and the contribution from other background processes as coloured histograms. Overflows are displayed in the last bin of each histogram. At the bottom, the ratio between prediction and data is displayed. Only statistical uncertainties are shown.

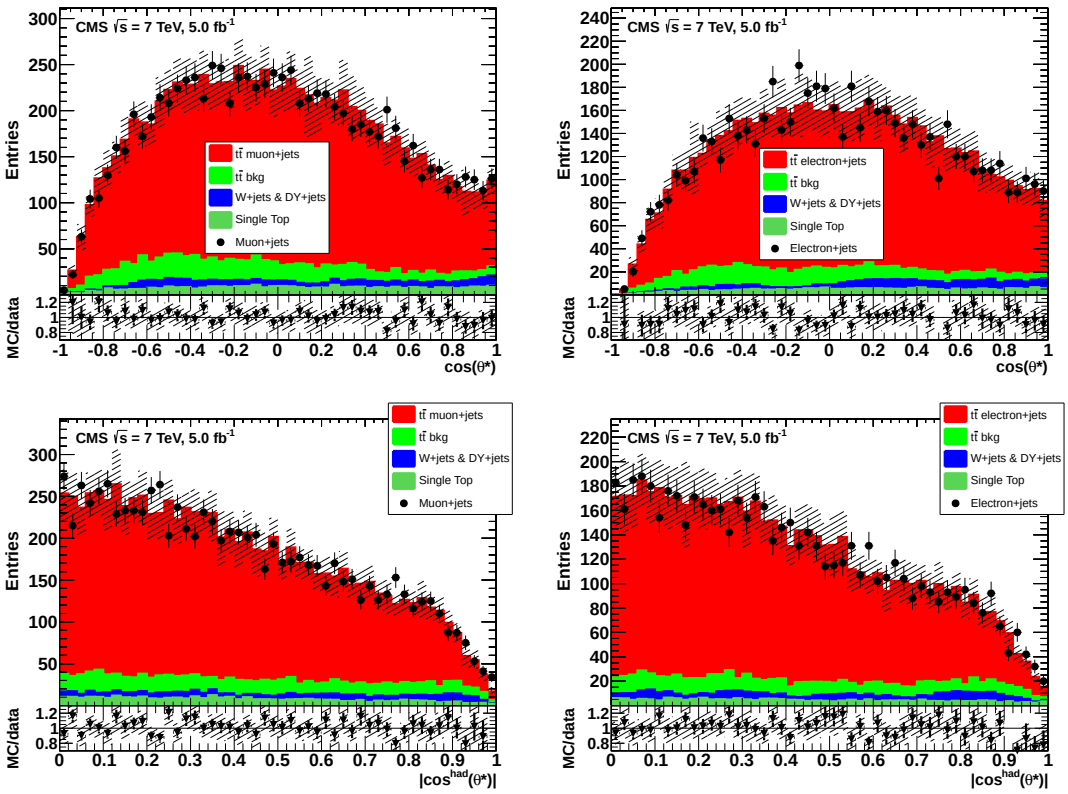

Figure 3: Cosine of the helicity angles $\cos\theta^*$(top) and $|\cos^{\text{had}}\theta^*|$ (bottom) for the muon+jets (left) and electron+jets (right) channels. Data are displayed as solid points, simulated $\mathrm{t\bar{t}}$ signal distributions as red histograms, and the contribution from other background processes as coloured histograms. At the bottom, the ratio between prediction and data is displayed. Systematic uncertainties are shown as hatched histograms.

in simulated events, so that their transverse momentum resolution is the same as measured in the data. The effect is propagated to the missing transverse energy, and the full analysis is repeated, similar to the procedure used to estimate the JES uncertainty.

Uncertainties in the lepton identification efficiency are investigated by varying the efficiency correction factor $\epsilon_\ell^{\text{DATA}}/\epsilon_\ell^{\text{MC}}$. In the case of muons, the efficiency correction factor depends on the η position of the muon in the detector. Since the measurement of the W-boson helicity is mainly affected by shape-dependent effects, uncertainties due to the muon efficiency correction factor are estimated by repeating the full analysis replacing the η-dependent factors by an uniform correction. In the case of electrons, only a very mild dependency on η is observed and the corresponding uncertainty, derived by assuming a flat η-dependence, has very little impact on the W-boson helicity measurement. Therefore, the efficiency correction factor for electron identification is shifted together with a shift in the scale factor for the jet component of the trigger according to the p_{T} and η position of the electrons and jets. The combination of electron and jet scale factors that lead to the maximum possible η-dependent effect is then applied and the full analysis is repeated.

The efficiencies for b tagging are measured using a control sample of multijet events [26], in data and simulation. The correction factors $\epsilon_{\text{b-tag}}^{\text{DATA}}/\epsilon_{\text{b-tag}}^{\text{MC}}$, which are applied to the simulated samples, are functions of the p_{T} and η of the jets, the number of the required b tags, as well as the number of heavy-flavour and light-flavour jets in the event. The scale factors are relatively

uniform in the typical p_T range of the selected jets, resulting in only a very small dependence of the W-boson helicity results on the b-tagging efficiency. The scale factors are varied by their uncertainties and the resulting differences are taken as a systematic uncertainty in the measured fractions.

The effect of pileup is estimated by varying the number of minimum bias collisions superimposed on each simulated signal event, according to an uncertainty of 5% which includes the uncertainties in the inelastic pp cross section, luminosity and other modelling uncertainties.

To account for a bias on the W-boson helicity measurement due to uncertainties in the normalisation from simulated background samples involving single top quarks, relative to the signal, the assumed reference cross sections are varied. While CMS has measured the single-top-quark production cross section in the t-channel with a 9% precision (67.2 ± 6.1 pb [37]), a systematic variation of $\pm 15\%$ is applied to cover the case of single-top-quark events produced with additional jets from radiation, which comprise the main contribution to this background component. Likewise, while CMS measures a cross section of 16^{+5}_{-4} pb [38] for the associated tW production case, the reference cross section used for the normalisation, 15.74 pb, is shifted by $\pm 40\%$. Finally, since the $\mathrm{t\bar{t}}$ sample normalisation is a free parameter in the helicity fits, the uncertainty associated with its initially assumed reference cross section does not affect the measurement.

The normalisation of the W+jets and DY+jets samples is estimated using the method described in Section 6 with an uncertainty of 100% and 30%, respectively. In both the W+jets and DY+jets events cases, the shapes of all relevant distributions in the simulation agree with the data and any systematic effects from variations in normalisations are much larger than any variations arising from shape; hence, systematic uncertainties due to possible differences in shape are negligible.

While the sample size for the reference simulated $\mathrm{t\bar{t}}$ dataset is chosen to be five times that of the processed data, it is possible for the reweighting method to introduce a systematic bias by degrading the statistical power of the simulated sample due to weights which can be larger than unity. Hence, special care must be taken to ensure that the statistical uncertainty of the MC prediction for each $\cos\theta^*_{\mathrm{rec}}$ bin is substantially smaller than the corresponding statistical uncertainty of the data. The uncertainties are estimated by repeating the analysis using a subsample of events that correspond to a fraction $1/N$ of the entire sample. The procedure is repeated many times, and the uncertainties on the W-boson helicity fractions taken as $\sigma/\sqrt{N}$ where σ is the spread observed on the fraction. Several values of N, between 2 and 10, are tested, and result in very similar uncertainties.

Since the W-boson helicity fractions depend directly on the top-quark mass, uncertainties in the latter could bias the measurement. This systematic effect is studied and taken into account, via $\mathrm{t\bar{t}}$ samples simulated using MADGRAPH for different m_t hypotheses. A variation of $\pm 1.4\,\mathrm{GeV}/c^2$ [29] about the assumed central value of $172.5\,\mathrm{GeV}/c^2$ is assumed.

Uncertainties on the helicity measurement from the choice of renormalisation and factorisation scales for the simulated signal samples are estimated using dedicated $\mathrm{t\bar{t}}$ simulated samples that vary the renormalisation and factorisation scales and the scale of the first emission in the parton shower, in a consistent manner, by factors of 0.5 and 2 with respect to a central value of Q, with $Q^2 = m_t^2c^2 + (\sum p_T^{\mathrm{jet}})^2$. The kinematic scale used to match jets to partons in the signal simulation is estimated using dedicated $\mathrm{t\bar{t}}$ samples where that matching parameter is varied by factors of 0.75 and 1.5 with respect to its central value of 40 GeV.

The systematic effects due to the PDFs used to simulate the signal and background samples

are estimated using two different methods [32], according to a reweighting technique. Firstly, events are reweighted using 100 members [39] of the NNPDF21 set [40], and the W-boson helicity fractions are remeasured for each of them. For a given helicity fraction, the RMS of the distribution of measurements from the different PDF members provides an uncertainty estimate that corresponds to 68% confidence level (CL). Secondly, the difference between the central values for CTEQ6L1 [16] (used in the analysis simulations) and MSTW2008lo68cl [31] is estimated. The systematic uncertainties in the measurements for the W-boson helicity fractions, due to intrinsic PDF uncertainties, are then taken as the largest difference between two different estimates.

The impact of all of the above systematic effects on the W-boson helicity fractions is detailed in Table 2, for the measurements for the leptonic side of the events ($\cos\theta^*$). The table shows results for the 3D and 2D fits, obtained by fitting two of the fractions or setting $F_R = 0$, respectively. Measurements using final states containing either a muon or an electron are presented in columns two through seven. The last three columns display systematic uncertainties for the combined measurements of the muon+jets and electron+jets channels, using the measurements from columns two through seven as inputs. The measurements are combined taking into account both statistical and systematic uncertainties. Common sources of uncertainties between the different measurements are assumed to be fully correlated. The dominant sources of systematic uncertainties in the leptonic side are the W+jets background normalisation, the signal modelling ($t\bar{t}$ renormalisation and factorization scales, and top-quark mass), and the statistics of the simulated samples.

Systematic uncertainties in the measurements for the hadronic branch, using the $|\cos^{\text{had}}\theta^*|$, are presented in Table 3. Since $|\cos^{\text{had}}\theta^*|$ has no sensitivity to a measurement of $F_L - F_R$, only the 2D fits are performed. Uncertainties on the individual measurements in the electron and muon channels are presented in the first two columns; in the last column, the combination of muons+jets and electrons+jets channels is shown. The hadronic branch is seen to have larger systematic uncertainties, compared with the leptonic branch, due, in part, to the dominant W+jets background and the importance of uncertainties from the JES and JER, as well as PDFs.

10 Results

The W-boson helicity fractions are measured according to the fits described in Section 7. The unitary condition $F_0 + F_L + F_R = 1$ is used to determine either (a) the right-handed fraction F_R from measurements of the free parameters, F_0 and F_L, in the 3D fits or (b) the left-handed fraction F_L from the measurement of the free parameter F_0 in the 2D fits assuming $F_R = 0$. Table 4 presents the fit measurement of each helicity parameter, one decay channel at a time, together with the statistical and systematic uncertainties. The statistical correlation factor $\rho_{0L}^{\text{stat.}}$ between F_0 and F_L is presented in the last column; the measurements are seen to be highly correlated. All measurements, from either the muon or electron channels, using either the leptonic or hadronic branches, are observed to be compatible within uncertainties. The measurements using the leptonic branch $\cos\theta^*$ are more precise, as expected.

Table 5 presents various combinations of the results presented in Table 4. Firstly, the muon+jets and electron+jets channels are combined using the leptonic branch measurements from the 3D fits. The χ^2 per degree of freedom for that combination is $0.109/2$, corresponding to a χ^2-probability of 94.7%. Secondly, the 2D fit measurements of the F_0 helicity fraction from the leptonic ($\cos\theta^*$) and hadronic ($\cos^{\text{had}}\theta^*$) branches are combined, separately for each decay channel. While the leptonic branch dominates with a weight of about 90%, the total uncertainty of the combination nevertheless decreases. Finally, the most precise measurement of

Table 2: Summary of the systematic uncertainties for the analysis using only the leptonic branch of the event, for the 3D fit, fitting F_0, F_L, and $\mathcal{F}_{t\bar{t}}$ (columns 2–3 for muon+jets analysis, 5–6 for electron+jets analysis, and 8–9 for the combination of both decay modes); and the 2D fit, fitting F_0 and $\mathcal{F}_{t\bar{t}}$ only (column 4 for muon+jets analysis, 7 for electron+jets analysis, and 10 for the combination of both decay modes). The numbers given correspond to the absolute uncertainty with respect to the central analysis: $\Delta F = (F^{\text{central}} - F^{\text{check}})$.

Systematic Uncertainties	μ+jets ($\cos\theta^*$)			e+jets ($\cos\theta^*$)			ℓ+jets ($\cos\theta^*$)		
	3D fit		2D fit	3D fit		2D fit	3D fit		2D fit
	$\pm\,\Delta F_0$	$\pm\,\Delta F_L$	$\pm\,\Delta F_0$	$\pm\,\Delta F_0$	$\pm\,\Delta F_L$	$\pm\,\Delta F_0$	$\pm\,\Delta F_0$	$\pm\,\Delta F_L$	$\pm\,\Delta F_0$
JES	0.005	0.003	0.001	0.006	0.002	0.003	0.006	0.003	0.001
JER	0.009	0.005	0.001	0.014	0.009	0.003	0.011	0.007	0.001
Lepton eff.	0.001	0.001	0.001	0.009	0.012	0.015	0.001	0.002	0.002
b-tag eff.	0.001	0.001	$< 10^{-3}$	$< 10^{-3}$	$< 10^{-3}$	0.001	0.001	$< 10^{-3}$	$< 10^{-3}$
Pileup	0.013	0.011	0.008	0.008	0.007	0.005	0.002	$< 10^{-3}$	0.008
Single-t bkg.	0.004	$< 10^{-3}$	0.003	0.004	$< 10^{-3}$	0.004	0.004	0.001	0.003
W+jets bkg.	0.019	0.007	0.006	0.009	0.006	0.022	0.013	0.004	0.006
DY+jets bkg.	0.002	0.001	0.001	0.001	$< 10^{-3}$	0.001	0.001	$< 10^{-3}$	0.001
MC statistics	0.016	0.012	0.009	0.019	0.015	0.012	0.016	0.012	0.010
Top-quark mass	0.011	0.008	0.007	0.025	0.018	0.014	0.016	0.011	0.019
$t\bar{t}$ scales	0.013	0.009	0.007	0.015	0.018	0.030	0.009	0.009	0.011
$t\bar{t}$ match. scale	0.004	0.001	0.006	0.010	0.013	0.016	0.011	0.010	0.008
PDF	0.002	0.001	0.003	0.004	0.002	0.002	0.002	$< 10^{-3}$	0.003

F_0 is obtained by subsequently combining the 2D fit measurements across the muon+jets and electron+jets channels, following the combination of the 2D fit measurements from the leptonic and hadronic branches.

Summaries of all measurements and their various combinations are presented in figures 4 and 5 for the 3D and 2D types of fits, respectively. All measurements are compatible with each other, and also compatible with the expectations from the SM [6].

11 Limits on anomalous couplings

The measured helicity fractions can be used to set limits on anomalous Wtb couplings. We assume the minimal parametrisation of the Wtb vertex suggested in Refs. [7, 8, 41] and as described in the introduction. We consider two specific scenarios. First, we assume $V_L = 1, V_R = g_L = 0$ and leave $\mathrm{Re}(g_R)$ as a free parameter. This CP-conserving scenario is particularly interesting because indirect constraints to g_R from radiative B-meson decay measurements are currently poor, $\mathrm{Re}(gR) \in [-0.15, +0.57]$ [42]. A specific feature of this scenario is that it does not provide any contribution to the right-handed helicity of the W boson, F_R. The grand combination of the longitudinal helicity fraction F_0 measurements, across both the leptonic and hadronic branches including both the muon and electron channels, and assuming $F_R = 0$, is reinterpreted in terms of $\mathrm{Re}(g_R)$, yielding

$$\mathrm{Re}(g_R) = -0.008 \pm 0.024\,(\text{stat.})^{+0.029}_{-0.030}\,(\text{syst.}),$$

which is consistent with the SM expectations within the quoted uncertainties. In quoting this result we have omitted another minimum of the fit closer to the $\mathrm{Re}(g_R) \approx 0.8$ region, which

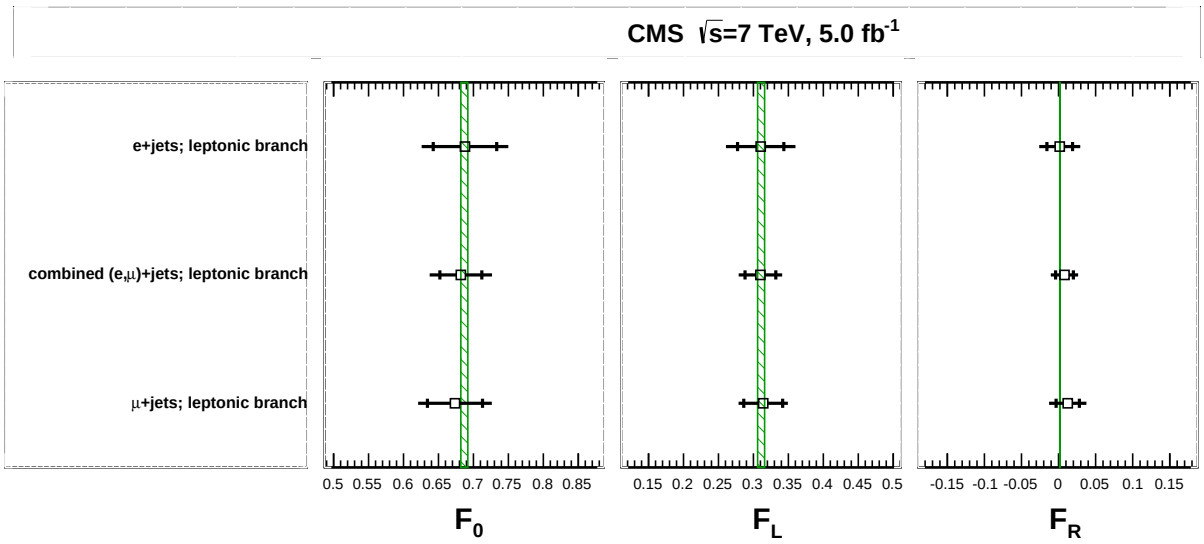

Figure 4: Summary of the W-boson helicity measurements in semileptonic decays of top-quark pairs with 2011 data for 3D fits. The inner error bars represent the statistical uncertainties and the outer error bars the statistical and systematic uncertainties, added in quadrature. NNLO predictions from Ref. [6] with their theoretical uncertainties are represented as hatched bands.

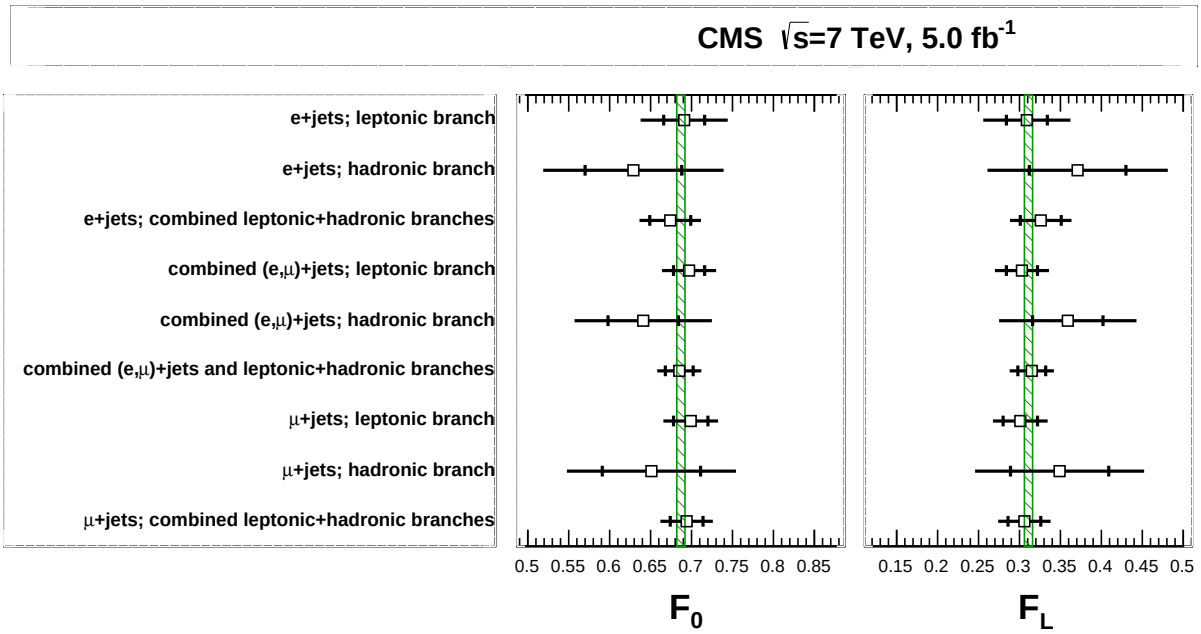

Figure 5: Summary of the W-boson helicity measurements in semileptonic decays of top-quark pairs with 2011 data, for 2D fits assuming $F_R = 0$. The inner error bars represent the statistical uncertainties and the outer error bars the statistical and systematic uncertainties, added in quadrature. NNLO predictions from Ref. [6] with their theoretical uncertainties are represented as hatched bands.

Table 3: Systematic uncertainties for the 2D fits using the hadronic branch of the $t\bar{t}$ system, and for the muon channel, electron channel, as well as the combination of both decay channels. The numbers given correspond to the absolute uncertainty with respect to the central analysis: $\Delta F = (F^{\text{central}} - F^{\text{check}})$.

Systematic Uncertainties	μ+jets ($\lvert\cos^{\text{had}}\theta^*\rvert$) 2D fit $\pm\,\Delta F_0$	e+jets ($\lvert\cos^{\text{had}}\theta^*\rvert$) 2D fit $\pm\,\Delta F_0$	ℓ+jets ($\lvert\cos^{\text{had}}\theta^*\rvert$) 2D fit $\pm\,\Delta F_0$
JES	0.010	0.008	0.002
JER	0.042	0.032	0.038
Lepton eff.	0.002	0.002	0.001
b-tag eff.	0.003	$< 10^{-3}$	0.002
Pileup	0.018	0.006	0.015
Single-t bkg.	0.005	0.007	0.006
W+jets bkg.	0.060	0.050	0.040
DY+jets bkg.	0.002	0.005	0.002
MC statistics	0.023	0.028	0.025
Top-quark mass	0.008	0.041	0.014
$t\bar{t}$ scales	0.022	0.033	0.027
$t\bar{t}$ match. scale	0.002	0.035	0.013
PDF	0.013	0.014	0.014

Table 4: Measurements of the W-boson helicity fractions from the $\cos\theta^*$(leptonic branch) and $\lvert\cos^{\text{had}}\theta^*\rvert$ (hadronic branch) distributions. The columns show the fit type, the decay channel, and the measurement of each helicity parameter, together with the statistical and systematic uncertainties. For the 3D fits, the last column presents the statistical correlation between F_0 and F_L, while for the 2D fit, total anticorrelation ($F_L = 1 - F_0$) is assumed.

Leptonic branch: $\cos\theta^*$					
Fit	Channel	$F_0 \pm$ (stat.) $\pm$ (syst.)	$F_L \pm$ (stat.) $\pm$ (syst.)	$F_R \pm$ (stat.) $\pm$ (syst.)	ρ_{0L}^{stat}
3D	μ+jets	0.674 $\pm$0.039$\pm$0.035	0.314 $\pm$0.028$\pm$0.022	0.012 $\pm$0.016$\pm$0.020	-0.95
3D	e+jets	0.688 $\pm$0.045$\pm$0.042	0.310 $\pm$0.033$\pm$0.037	0.002 $\pm$0.017$\pm$0.023	-0.95
2D	μ+jets	0.698 $\pm$0.021$\pm$0.019	0.302 $\pm$0.021$\pm$0.019	fixed at 0	-1
2D	e+jets	0.691 $\pm$0.025$\pm$0.047	0.309 $\pm$0.025$\pm$0.047	fixed at 0	-1
Hadronic branch: $\lvert\cos^{\text{had}}\theta^*\rvert$					
Fit	Channel	$F_0 \pm$ (stat.) $\pm$ (syst.)	$F_L \pm$ (stat.) $\pm$ (syst.)	$F_R \pm$ (stat.) $\pm$ (syst.)	ρ_{0L}
2D	μ+jets	0.651 $\pm$0.060$\pm$0.084	0.349 $\pm$0.060$\pm$0.084	fixed at 0	-1
2D	e+jets	0.629 $\pm$0.060$\pm$0.093	0.371 $\pm$0.060$\pm$0.093	fixed at 0	-1

would lead to an increase of almost a factor of three in the single-top-quark cross section [43], which would not be consistent with the recent CMS measurement [37]. In terms of the effective dimension-six Lagrangian $\mathcal{O}_{uW}^{33}$ defined in Refs. [7, 8] we obtain the equivalent result,

$$\text{Re}(C_{uW}^{33})/\Lambda^2 = -0.088 \pm 0.280\,(\text{stat.})^{+0.339}_{-0.352}\,(\text{syst.})\,\text{TeV}^{-2},$$

where Λ is the scale of new physics and $\text{Re}(C_{uW}^{33})$ the effective operator coefficient.

In the second scenario, again assuming CP is conserved, we choose $\text{Re}(g_L)$ and $\text{Re}(g_R)$ as free parameters of the fit. Limits on those parameters are determined using the combined measurements of the muon+jets and electron+jets channels from the 3D fit of the leptonic branch, $\cos\theta^*$. The results of the likelihood fit for the parameters F_0 and F_L can reinterpreted in terms

Table 5: The combined helicity fractions and their uncertainties, including the type of fit performed, the channels (ℓ = e, μ combination) and branches of the $t\bar{t}$ system ("l" for leptonic, $\cos\theta^*$, and "h" for hadronic, $|\cos^{had}\theta^*|$) used in the combination, as well as the total correlation between F_0 and F_L.

Fit	Channel(s)	Branch	Fraction ± (stat.) ± (syst.) [total]		ρ_{0L}^{total}
3D	ℓ+jets	l	F_0	0.682 ±0.030±0.033 [0.045]	−0.95
			F_L	0.310 ±0.022±0.022 [0.032]	
			F_R	0.008 ±0.012±0.014 [0.018]	
2D	μ+jets	l+h	F_0	0.694 ±0.020±0.025 [0.032]	−1
			F_L	0.306 ±0.020±0.025 [0.032]	
2D	e+jets	l+h	F_0	0.674 ±0.025±0.028 [0.037]	−1
			F_L	0.326 ±0.025±0.028 [0.037]	
2D	ℓ+jets	l+h	F_0	0.685 ±0.017±0.021 [0.027]	−1
			F_L	0.315 ±0.017±0.021 [0.027]	

of the parameters $\mathrm{Re}(g_L)$ and $\mathrm{Re}(g_R)$. Figure 6 shows the regions of the $\mathrm{Re}(g_L)$, $\mathrm{Re}(g_R)$ plane allowed at 68% and 95% CL. As in the first scenario, a region near $\mathrm{Re}(g_L) = 0$ and $\mathrm{Re}(g_R) \gg 0$, allowed by the fit but excluded by the CMS single-top quark measurement, is not shown.

The result obtained from the first scenario represents an improvement of about 50% on the precision of $\mathrm{Re}(g_R)$ with respect to previous measurements [4], while the limits from the second scenario are similar to those from Ref. [4].

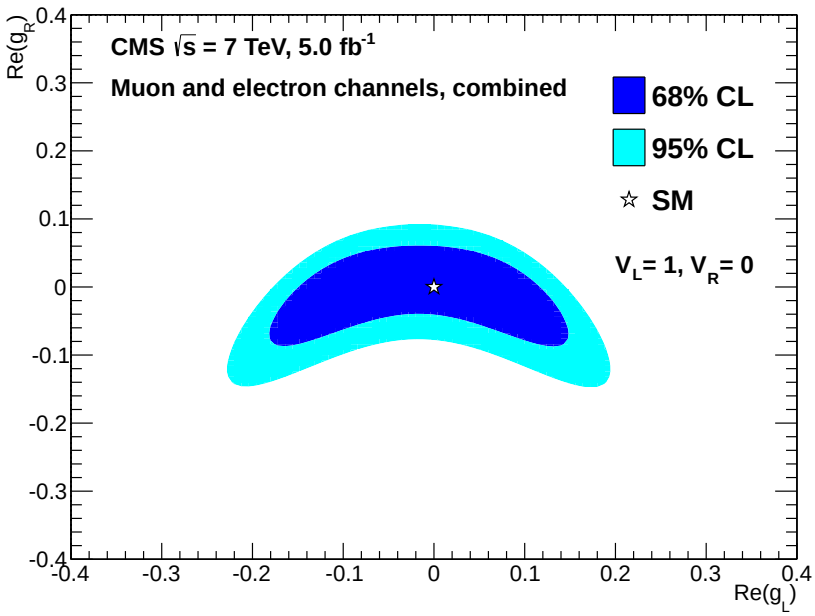

Figure 6: Limits on the real components of the anomalous couplings g_L, g_R at 68% and 95% CL, for $V_L = 1$ and $V_R = 0$. The SM prediction ($g_R = 0$ and $g_L = 0$) is also shown.

12 Summary

The W-boson helicity has been measured in top-quark-pair events decaying semileptonically, both in the muon+jets and in the electron+jets channels, using proton-proton collisions data at $\sqrt{s} = 7\,\text{TeV}$, corresponding to an integrated luminosity of $5.0\,\text{fb}^{-1}$. Both the leptonic and the hadronic branches of the decay have been studied. The most precise measurement, not constraining F_R to the SM, corresponding to the combination of muon and electron channels, using only the leptonic branch, yields:

$$\begin{aligned} F_0 &= 0.682 \pm 0.030\,(\text{stat.}) \pm 0.033\,(\text{syst.}), \\ F_L &= 0.310 \pm 0.022\,(\text{stat.}) \pm 0.022\,(\text{syst.}), \\ F_R &= 0.008 \pm 0.012\,(\text{stat.}) \pm 0.014\,(\text{syst.}), \end{aligned}$$

with a correlation coefficient of -0.95 between F_0 and F_L.

The measured W-boson helicity fractions are in agreement with the predictions from the standard model. Assuming a minimal parametrisation of the Wtb vertex, stringent limits on the real components of the anomalous couplings g_L and g_R are also derived.

Acknowledgements

We congratulate our colleagues in the CERN accelerator departments for the excellent performance of the LHC and thank the technical and administrative staffs at CERN and at other CMS institutes for their contributions to the success of the CMS effort. In addition, we gratefully acknowledge the computing centres and personnel of the Worldwide LHC Computing Grid for delivering so effectively the computing infrastructure essential to our analyses. Finally, we acknowledge the enduring support for the construction and operation of the LHC and the CMS detector provided by the following funding agencies: the Austrian Federal Ministry of Science and Research and the Austrian Science Fund; the Belgian Fonds de la Recherche Scientifique, and Fonds voor Wetenschappelijk Onderzoek; the Brazilian Funding Agencies (CNPq, CAPES, FAPERJ, and FAPESP); the Bulgarian Ministry of Education and Science; CERN; the Chinese Academy of Sciences, Ministry of Science and Technology, and National Natural Science Foundation of China; the Colombian Funding Agency (COLCIENCIAS); the Croatian Ministry of Science, Education and Sport; the Research Promotion Foundation, Cyprus; the Ministry of Education and Research, Recurrent financing contract SF0690030s09 and European Regional Development Fund, Estonia; the Academy of Finland, Finnish Ministry of Education and Culture, and Helsinki Institute of Physics; the Institut National de Physique Nucléaire et de Physique des Particules / CNRS, and Commissariat à l'Énergie Atomique et aux Énergies Alternatives / CEA, France; the Bundesministerium für Bildung und Forschung, Deutsche Forschungsgemeinschaft, and Helmholtz-Gemeinschaft Deutscher Forschungszentren, Germany; the General Secretariat for Research and Technology, Greece; the National Scientific Research Foundation, and National Office for Research and Technology, Hungary; the Department of Atomic Energy and the Department of Science and Technology, India; the Institute for Studies in Theoretical Physics and Mathematics, Iran; the Science Foundation, Ireland; the Istituto Nazionale di Fisica Nucleare, Italy; the Korean Ministry of Education, Science and Technology and the World Class University program of NRF, Republic of Korea; the Lithuanian Academy of Sciences; the Mexican Funding Agencies (CINVESTAV, CONACYT, SEP, and UASLP-FAI); the Ministry of Science and Innovation, New Zealand; the Pakistan Atomic Energy Commission; the Ministry of Science and Higher Education and the National Science Centre, Poland; the Fundação para a Ciência e a Tecnologia, Portugal; JINR, Dubna; the Ministry of Education

and Science of the Russian Federation, the Federal Agency of Atomic Energy of the Russian Federation, Russian Academy of Sciences, and the Russian Foundation for Basic Research; the Ministry of Education, Science and Technological Development of Serbia; the Secretaría de Estado de Investigación, Desarrollo e Innovación and Programa Consolider-Ingenio 2010, Spain; the Swiss Funding Agencies (ETH Board, ETH Zurich, PSI, SNF, UniZH, Canton Zurich, and SER); the National Science Council, Taipei; the Thailand Center of Excellence in Physics, the Institute for the Promotion of Teaching Science and Technology of Thailand, Special Task Force for Activating Research and the National Science and Technology Development Agency of Thailand; the Scientific and Technical Research Council of Turkey, and Turkish Atomic Energy Authority; the Science and Technology Facilities Council, UK; the US Department of Energy, and the US National Science Foundation. Individuals have received support from the Marie-Curie programme and the European Research Council and EPLANET (European Union); the Leventis Foundation; the A. P. Sloan Foundation; the Alexander von Humboldt Foundation; the Belgian Federal Science Policy Office; the Fonds pour la Formation à la Recherche dans l'Industrie et dans l'Agriculture (FRIA-Belgium); the Agentschap voor Innovatie door Wetenschap en Technologie (IWT-Belgium); the Ministry of Education, Youth and Sports (MEYS) of Czech Republic; the Council of Science and Industrial Research, India; the Compagnia di San Paolo (Torino); the HOMING PLUS programme of Foundation for Polish Science, cofinanced by EU, Regional Development Fund; and the Thalis and Aristeia programmes cofinanced by EU-ESF and the Greek NSRF.

References

[1] CDF Collaboration, "Observation of top quark production in $\bar{p}p$ collisions", *Phys. Rev. Lett.* **74** (1995) 2626, doi:10.1103/PhysRevLett.74.2626, arXiv:hep-ex/9503002.

[2] D0 Collaboration, "Observation of the top quark", *Phys. Rev. Lett.* **74** (1995) 2632, doi:10.1103/PhysRevLett.74.2632, arXiv:hep-ex/9503003.

[3] CDF and D0 Collaborations, "Combination of CDF and D0 measurements of the W boson helicity in top quark decays", *Phys. Rev. D* **85** (2012) 071106, doi:10.1103/PhysRevD.85.071106, arXiv:1202.5272.

[4] ATLAS Collaboration, "Measurement of the W boson polarization in top quark decays with the ATLAS detector", *JHEP* **06** (2012) 088, doi:10.1007/JHEP06(2012)088, arXiv:1205.2484.

[5] J. G. K. M. Fischer, S. Groote and M. C. Mauser, "Longitudinal, transverse-plus and transverse-minus W bosons in unpolarized top quark decays at $\mathcal{O}(\alpha_s)$", *Phys. Rev. D* **63** (2001) 031501(R), doi:10.1103/PhysRevD.63.031501, arXiv:hep-ph/0011075.

[6] A. Czarnecki, J. G. Korner, and J. H. Piclum, "Helicity fractions of W bosons from top quark decays at NNLO in QCD", *Phys. Rev. D* **81** (2010) 111503, doi:10.1103/PhysRevD.81.111503, arXiv:1005.2625.

[7] J. A. Aguilar-Saavedra, "A minimal set of top anomalous couplings", *Nucl. Phys. B* **812** (2009) 181, doi:10.1016/j.nuclphysb.2008.12.012, arXiv:0811.3842.

[8] J. A. Aguilar-Saavedra, "A minimal set of top-Higgs anomalous couplings", *Nucl. Phys. B* **821** (2009) 215, doi:10.1016/j.nuclphysb.2009.06.022, arXiv:0904.2387.

[9] J. A. Aguilar-Saavedra and J. Bernabeu, "W polarisation beyond helicity fractions in top quark decays", *Nucl. Phys. B* **840** (2010) 349, doi:10.1016/j.nuclphysb.2010.07.012, arXiv:1005.5382.

[10] CMS Collaboration, "The CMS experiment at the CERN LHC", *JINST* **3** (2008) S08004, doi:10.1088/1748-0221/3/08/S08004.

[11] CMS Collaboration, "Absolute Calibration of the Luminosity Measurement at CMS: Winter 2012 Update", CMS Physics Analysis Summary CMS-PAS-SMP-12-008, (2012).

[12] J. Alwall et al., "MadGraph 5: going beyond", *JHEP* **1106** (2011) 128, doi:10.1007/JHEP06(2011)128, arXiv:1106.0522.

[13] T. Sjöstrand, S. Mrenna, and P. Z. Skands, "PYTHIA 6.4 physics and manual", *JHEP* **05** (2006) 026, doi:10.1088/1126-6708/2006/05/026, arXiv:hep-ph/0603175.

[14] N. Davidson et al., "Universal Interface of TAUOLA: Technical and physics documentation", *Comput. Phys. Commun.* **183** (2012) 821, doi:10.1016/j.cpc.2011.12.009, arXiv:1002.0543.

[15] C. O. S. Alioli, P. Nason and E. Re, "NLO vector-boson production matched with shower in POWHEG", *JHEP* **07** (2008) 060, doi:10.1088/1126-6708/2008/07/060, arXiv:0805.4802.

[16] J. Pumplin et al., "New Generation of Parton Distributions with Uncertainties from Global QCD Analysis", *JHEP* **07** (2002) 012, doi:10.1088/1126-6708/2002/07/012, arXiv:hep-ex/0201195.

[17] H.-L. Lai et al., "New parton distributions for collider physics", *Phys. Rev. D* **82** (2010) 074024, doi:10.1103/PhysRevD.82.074024, arXiv:1007.2241.

[18] CMS Collaboration, "Particle–Flow Event Reconstruction in CMS and Performance for Jets, Taus, and $E_{\mathrm{T}}^{\mathrm{miss}}$", CMS Physics Analysis Summary CMS-PAS-PFT-09-001.

[19] CMS Collaboration, "Jet Performance in pp Collisions at $\sqrt{s}$=7 TeV", CMS Physics Analysis Summary CMS-PAS-JME-10-003, (2010).

[20] CMS Collaboration, "Measurement of the $\mathrm{t\bar{t}}$ production cross section in pp collisions at $\sqrt{s} = 7$ TeV using the kinematic properties of events with leptons and jets", *Eur. Phys. J. C* **71** (2011) 1721, doi:10.1140/epjc/s10052-011-1721-3.

[21] CMS Collaboration, "Electron Reconstruction and Identification at $\sqrt{s} = 7$ TeV", CMS Physics Analysis Summary CMS-PAS-EGM-10-004, (2010).

[22] M. Cacciari, G. P. Salam, and G. Soyez, "The anti-k_{T} jet clustering algorithm", *JHEP* **04** (2008) 063, doi:10.1088/1126-6708/2008/04/063, arXiv:0802.1189.

[23] M. Cacciari, G. P. Salam, and G. Soyez, "FastJet User Manual", *Eur. Phys. J. C* **72** (2012) 1896, doi:10.1140/epjc/s10052-012-1896-2, arXiv:1111.6097.

[24] CMS Collaboration, "Determination of jet energy calibration and transverse momentum resolution in CMS", *JINST* **6** (2011) P11002, doi:10.1088/1748-0221/6/11/P11002.

[25] CMS Collaboration, "Missing transverse energy performance of the CMS detector", *JINST* **6** (2011) 09001, doi:10.1088/1748-0221/6/09/P09001, arXiv:1106.5048.

[26] CMS Collaboration, "Identification of b-quark jets with the CMS experiment", *JINST* **8** (2013) P04013, doi:10.1088/1748-0221/8/04/P04013, arXiv:1211.4462.

[27] CMS Collaboration, "Measurements of inclusive W and Z cross sections in pp collisions at $\sqrt{s}$ = 7 TeV", *JHEP* **01** (2010) 080, doi:10.1007/JHEP01(2011)080.

[28] Particle Data Group, J. Beringer et al., "2012 Review of Particle Physics", *Phys. Rev. D* **86** (2012) 010001, doi:10.1103/PhysRevD.86.010001.

[29] ATLAS, CDF, CMS and D0 Collaborations, "Combination of the top-quark mass measurements from the Tevatron and from the LHC colliders", (2013). arXiv:1302.0830.

[30] R. Gavin, Y. Li, F. Petriello, and S. Quackenbush, "FEWZ 2.0: A code for hadronic Z production at next-to-next-to-leading order", *Comput. Phys. Commun.* **182** (2011) 2388, doi:10.1016/j.cpc.2011.06.008, arXiv:1011.3540.

[31] A. D. Martin, W. J. Stirling, R. S. Thorne, and G. Watt, "Parton distributions for the LHC", *Eur. Phys. J. C* **63** (2009) 189, doi:10.1140/epjc/s10052-009-1072-5, arXiv:0901.0002.

[32] M. Botje et al., "The PDF4LHC Working Group Interim Recommendations", (2011). arXiv:1101.0538.

[33] CDF Collaboration, "Measurement of the W-boson helicity fractions in top-quark decays using $\cos(\theta^*)$", *Phys. Lett. B* **674** (2009) 160, doi:10.1016/j.physletb.2009.02.040, arXiv:0811.0344.

[34] D0 Collaboration, "Measurement of the W boson helicity in top quark decays using 5.4 fb^{-1} of $\text{p}\bar{\text{p}}$ collision data", *Phys. Rev. D* **83** (2011) 032009, doi:10.1103/PhysRevD.83.032009, arXiv:1011.6549.

[35] N. Kidonakis, "Next-to-next-to-leading-order collinear and soft gluon corrections for *t*-channel single top quark production", *Phys. Rev. D* **83** (2011) 091503, doi:10.1103/PhysRevD.83.091503, arXiv:1103.2792.

[36] N. Kidonakis, "Two-loop soft anomalous dimensions for single top quark associated production with a W^- or H^-", *Phys. Rev. D* **82** (2010) 054018, doi:10.1103/PhysRevD.82.054018, arXiv:1005.4451.

[37] CMS Collaboration, "Measurement of the single-top-quark *t*-channel cross section in pp collisions at $\sqrt{s} = 7$ TeV", *JHEP* **12** (2012) 036, doi:10.1007/JHEP06(2013)081, arXiv:1303.4571.

[38] CMS Collaboration, "Evidence for Associated Production of a Single Top Quark and W Boson in pp Collisions at $\sqrt{s} = 7$ TeV", *Phys. Rev. Lett.* **110** (2013) 022003, doi:10.1103/PhysRevLett.110.022003, arXiv:1209.3489.

[39] M. R. Whalley, D. Bourilkov, and R. C. Group, "The Les Houches Accord PDFs (LHAPDF) and Lhaglue", (2005). arXiv:hep-ph/0508110.

[40] NNPDF Collaboration, "Impact of heavy quark masses on parton distributions and LHC phenomenology", *Nucl. Phys. B* **849** (2011) 296, doi:10.1016/j.nuclphysb.2011.03.021, arXiv:1101.1300.

[41] J. A. Aguilar-Saavedra et al., "Probing anomalous Wtb couplings in top pair decays", *Eur. Phys. J. C* **50** (2007) 519, doi:10.1140/epjc/s10052-007-0289-4, arXiv:hep-ph/0605190.

[42] B. Grzadkowski and M. Misiak, "Anomalous Wtb coupling effects in the weak radiative B-meson decay", *Phys. Rev. D* **78** (2008) 077501, doi:10.1103/PhysRevD.78.077501, arXiv:0802.1413. Erratum in doi:10.1103/PhysRevD.84.059903.

[43] J. A. Aguilar-Saavedra, "Single top quark production at LHC with anomalous Wtb couplings", *Nucl. Phys. B* **804** (2008) 160, doi:10.1016/j.nuclphysb.2008.06.013, arXiv:0803.3810.

A The CMS Collaboration

Yerevan Physics Institute, Yerevan, Armenia
S. Chatrchyan, V. Khachatryan, A.M. Sirunyan, A. Tumasyan

Institut für Hochenergiephysik der OeAW, Wien, Austria
W. Adam, T. Bergauer, M. Dragicevic, J. Erö, C. Fabjan[1], M. Friedl, R. Frühwirth[1], V.M. Ghete, N. Hörmann, J. Hrubec, M. Jeitler[1], W. Kiesenhofer, V. Knünz, M. Krammer[1], I. Krätschmer, D. Liko, I. Mikulec, D. Rabady[2], B. Rahbaran, C. Rohringer, H. Rohringer, R. Schöfbeck, J. Strauss, A. Taurok, W. Treberer-Treberspurg, W. Waltenberger, C.-E. Wulz[1]

National Centre for Particle and High Energy Physics, Minsk, Belarus
V. Mossolov, N. Shumeiko, J. Suarez Gonzalez

Universiteit Antwerpen, Antwerpen, Belgium
S. Alderweireldt, M. Bansal, S. Bansal, T. Cornelis, E.A. De Wolf, X. Janssen, A. Knutsson, S. Luyckx, L. Mucibello, S. Ochesanu, B. Roland, R. Rougny, Z. Staykova, H. Van Haevermaet, P. Van Mechelen, N. Van Remortel, A. Van Spilbeeck

Vrije Universiteit Brussel, Brussel, Belgium
F. Blekman, S. Blyweert, J. D'Hondt, A. Kalogeropoulos, J. Keaveney, M. Maes, A. Olbrechts, S. Tavernier, W. Van Doninck, P. Van Mulders, G.P. Van Onsem, I. Villella

Université Libre de Bruxelles, Bruxelles, Belgium
C. Caillol, B. Clerbaux, G. De Lentdecker, L. Favart, A.P.R. Gay, T. Hreus, A. Léonard, P.E. Marage, A. Mohammadi, L. Perniè, T. Reis, T. Seva, L. Thomas, C. Vander Velde, P. Vanlaer, J. Wang

Ghent University, Ghent, Belgium
V. Adler, K. Beernaert, L. Benucci, A. Cimmino, S. Costantini, S. Dildick, G. Garcia, B. Klein, J. Lellouch, A. Marinov, J. Mccartin, A.A. Ocampo Rios, D. Ryckbosch, M. Sigamani, N. Strobbe, F. Thyssen, M. Tytgat, S. Walsh, E. Yazgan, N. Zaganidis

Université Catholique de Louvain, Louvain-la-Neuve, Belgium
S. Basegmez, C. Beluffi[3], G. Bruno, R. Castello, A. Caudron, L. Ceard, G.G. Da Silveira, C. Delaere, T. du Pree, D. Favart, L. Forthomme, A. Giammanco[4], J. Hollar, P. Jez, V. Lemaitre, J. Liao, O. Militaru, C. Nuttens, D. Pagano, A. Pin, K. Piotrzkowski, A. Popov[5], M. Selvaggi, J.M. Vizan Garcia

Université de Mons, Mons, Belgium
N. Beliy, T. Caebergs, E. Daubie, G.H. Hammad

Centro Brasileiro de Pesquisas Fisicas, Rio de Janeiro, Brazil
G.A. Alves, M. Correa Martins Junior, T. Martins, M.E. Pol, M.H.G. Souza

Universidade do Estado do Rio de Janeiro, Rio de Janeiro, Brazil
W.L. Aldá Júnior, W. Carvalho, J. Chinellato[6], A. Custódio, E.M. Da Costa, D. De Jesus Damiao, C. De Oliveira Martins, S. Fonseca De Souza, H. Malbouisson, M. Malek, D. Matos Figueiredo, L. Mundim, H. Nogima, W.L. Prado Da Silva, A. Santoro, A. Sznajder, E.J. Tonelli Manganote[6], A. Vilela Pereira

Universidade Estadual Paulista [a], Universidade Federal do ABC [b], São Paulo, Brazil
C.A. Bernardes[b], F.A. Dias[a,7], T.R. Fernandez Perez Tomei[a], E.M. Gregores[b], C. Lagana[a], P.G. Mercadante[b], S.F. Novaes[a], Sandra S. Padula[a]

Institute for Nuclear Research and Nuclear Energy, Sofia, Bulgaria
V. Genchev[2], P. Iaydjiev[2], S. Piperov, M. Rodozov, G. Sultanov, M. Vutova

University of Sofia, Sofia, Bulgaria
A. Dimitrov, R. Hadjiiska, V. Kozhuharov, L. Litov, B. Pavlov, P. Petkov

Institute of High Energy Physics, Beijing, China
J.G. Bian, G.M. Chen, H.S. Chen, C.H. Jiang, D. Liang, S. Liang, X. Meng, J. Tao, X. Wang, Z. Wang, H. Xiao

State Key Laboratory of Nuclear Physics and Technology, Peking University, Beijing, China
C. Asawatangtrakuldee, Y. Ban, Y. Guo, Q. Li, W. Li, S. Liu, Y. Mao, S.J. Qian, D. Wang, L. Zhang, W. Zou

Universidad de Los Andes, Bogota, Colombia
C. Avila, C.A. Carrillo Montoya, L.F. Chaparro Sierra, J.P. Gomez, B. Gomez Moreno, J.C. Sanabria

Technical University of Split, Split, Croatia
N. Godinovic, D. Lelas, R. Plestina[8], D. Polic, I. Puljak

University of Split, Split, Croatia
Z. Antunovic, M. Kovac

Institute Rudjer Boskovic, Zagreb, Croatia
V. Brigljevic, K. Kadija, J. Luetic, D. Mekterovic, S. Morovic, L. Tikvica

University of Cyprus, Nicosia, Cyprus
A. Attikis, G. Mavromanolakis, J. Mousa, C. Nicolaou, F. Ptochos, P.A. Razis

Charles University, Prague, Czech Republic
M. Finger, M. Finger Jr.

Academy of Scientific Research and Technology of the Arab Republic of Egypt, Egyptian Network of High Energy Physics, Cairo, Egypt
Y. Assran[9], S. Elgammal[10], A. Ellithi Kamel[11], A.M. Kuotb Awad[12], M.A. Mahmoud[12], A. Radi[13,14]

National Institute of Chemical Physics and Biophysics, Tallinn, Estonia
M. Kadastik, M. Müntel, M. Murumaa, M. Raidal, L. Rebane, A. Tiko

Department of Physics, University of Helsinki, Helsinki, Finland
P. Eerola, G. Fedi, M. Voutilainen

Helsinki Institute of Physics, Helsinki, Finland
J. Härkönen, V. Karimäki, R. Kinnunen, M.J. Kortelainen, T. Lampén, K. Lassila-Perini, S. Lehti, T. Lindén, P. Luukka, T. Mäenpää, T. Peltola, E. Tuominen, J. Tuominiemi, E. Tuovinen, L. Wendland

Lappeenranta University of Technology, Lappeenranta, Finland
T. Tuuva

DSM/IRFU, CEA/Saclay, Gif-sur-Yvette, France
M. Besancon, F. Couderc, M. Dejardin, D. Denegri, B. Fabbro, J.L. Faure, F. Ferri, S. Ganjour, A. Givernaud, P. Gras, G. Hamel de Monchenault, P. Jarry, E. Locci, J. Malcles, L. Millischer, A. Nayak, J. Rander, A. Rosowsky, M. Titov

Laboratoire Leprince-Ringuet, Ecole Polytechnique, IN2P3-CNRS, Palaiseau, France
S. Baffioni, F. Beaudette, L. Benhabib, M. Bluj[15], P. Busson, C. Charlot, N. Daci, T. Dahms, M. Dalchenko, L. Dobrzynski, A. Florent, R. Granier de Cassagnac, M. Haguenauer, P. Miné, C. Mironov, I.N. Naranjo, M. Nguyen, C. Ochando, P. Paganini, D. Sabes, R. Salerno, Y. Sirois, C. Veelken, A. Zabi

Institut Pluridisciplinaire Hubert Curien, Université de Strasbourg, Université de Haute Alsace Mulhouse, CNRS/IN2P3, Strasbourg, France
J.-L. Agram[16], J. Andrea, D. Bloch, J.-M. Brom, E.C. Chabert, C. Collard, E. Conte[16], F. Drouhin[16], J.-C. Fontaine[16], D. Gelé, U. Goerlach, C. Goetzmann, P. Juillot, A.-C. Le Bihan, P. Van Hove

Centre de Calcul de l'Institut National de Physique Nucleaire et de Physique des Particules, CNRS/IN2P3, Villeurbanne, France
S. Gadrat

Université de Lyon, Université Claude Bernard Lyon 1, CNRS-IN2P3, Institut de Physique Nucléaire de Lyon, Villeurbanne, France
S. Beauceron, N. Beaupere, G. Boudoul, S. Brochet, J. Chasserat, R. Chierici, D. Contardo, P. Depasse, H. El Mamouni, J. Fay, S. Gascon, M. Gouzevitch, B. Ille, T. Kurca, M. Lethuillier, L. Mirabito, S. Perries, L. Sgandurra, V. Sordini, M. Vander Donckt, P. Verdier, S. Viret

Institute of High Energy Physics and Informatization, Tbilisi State University, Tbilisi, Georgia
Z. Tsamalaidze[17]

RWTH Aachen University, I. Physikalisches Institut, Aachen, Germany
C. Autermann, S. Beranek, B. Calpas, M. Edelhoff, L. Feld, N. Heracleous, O. Hindrichs, K. Klein, A. Ostapchuk, A. Perieanu, F. Raupach, J. Sammet, S. Schael, D. Sprenger, H. Weber, B. Wittmer, V. Zhukov[5]

RWTH Aachen University, III. Physikalisches Institut A, Aachen, Germany
M. Ata, J. Caudron, E. Dietz-Laursonn, D. Duchardt, M. Erdmann, R. Fischer, A. Güth, T. Hebbeker, C. Heidemann, K. Hoepfner, D. Klingebiel, S. Knutzen, P. Kreuzer, M. Merschmeyer, A. Meyer, M. Olschewski, K. Padeken, P. Papacz, H. Pieta, H. Reithler, S.A. Schmitz, L. Sonnenschein, J. Steggemann, D. Teyssier, S. Thüer, M. Weber

RWTH Aachen University, III. Physikalisches Institut B, Aachen, Germany
V. Cherepanov, Y. Erdogan, G. Flügge, H. Geenen, M. Geisler, W. Haj Ahmad, F. Hoehle, B. Kargoll, T. Kress, Y. Kuessel, J. Lingemann[2], A. Nowack, I.M. Nugent, L. Perchalla, O. Pooth, A. Stahl

Deutsches Elektronen-Synchrotron, Hamburg, Germany
I. Asin, N. Bartosik, J. Behr, W. Behrenhoff, U. Behrens, A.J. Bell, M. Bergholz[18], A. Bethani, K. Borras, A. Burgmeier, A. Cakir, L. Calligaris, A. Campbell, S. Choudhury, F. Costanza, C. Diez Pardos, S. Dooling, T. Dorland, G. Eckerlin, D. Eckstein, G. Flucke, A. Geiser, I. Glushkov, A. Grebenyuk, P. Gunnellini, S. Habib, J. Hauk, G. Hellwig, D. Horton, H. Jung, M. Kasemann, P. Katsas, C. Kleinwort, H. Kluge, M. Krämer, D. Krücker, E. Kuznetsova, W. Lange, J. Leonard, K. Lipka, W. Lohmann[18], B. Lutz, R. Mankel, I. Marfin, I.-A. Melzer-Pellmann, A.B. Meyer, J. Mnich, A. Mussgiller, S. Naumann-Emme, O. Novgorodova, F. Nowak, J. Olzem, H. Perrey, A. Petrukhin, D. Pitzl, R. Placakyte, A. Raspereza, P.M. Ribeiro Cipriano, C. Riedl, E. Ron, M.Ö. Sahin, J. Salfeld-Nebgen, R. Schmidt[18], T. Schoerner-Sadenius, N. Sen, M. Stein, R. Walsh, C. Wissing

University of Hamburg, Hamburg, Germany
M. Aldaya Martin, V. Blobel, H. Enderle, J. Erfle, E. Garutti, U. Gebbert, M. Görner, M. Gosselink, J. Haller, K. Heine, R.S. Höing, G. Kaussen, H. Kirschenmann, R. Klanner, R. Kogler, J. Lange, I. Marchesini, T. Peiffer, N. Pietsch, D. Rathjens, C. Sander, H. Schettler, P. Schleper, E. Schlieckau, A. Schmidt, M. Schröder, T. Schum, M. Seidel, J. Sibille[19], V. Sola, H. Stadie, G. Steinbrück, J. Thomsen, D. Troendle, E. Usai, L. Vanelderen

Institut für Experimentelle Kernphysik, Karlsruhe, Germany
C. Barth, C. Baus, J. Berger, C. Böser, E. Butz, T. Chwalek, W. De Boer, A. Descroix, A. Dierlamm, M. Feindt, M. Guthoff[2], F. Hartmann[2], T. Hauth[2], H. Held, K.H. Hoffmann, U. Husemann, I. Katkov[5], J.R. Komaragiri, A. Kornmayer[2], P. Lobelle Pardo, D. Martschei, Th. Müller, M. Niegel, A. Nürnberg, O. Oberst, J. Ott, G. Quast, K. Rabbertz, F. Ratnikov, S. Röcker, F.-P. Schilling, G. Schott, H.J. Simonis, F.M. Stober, R. Ulrich, J. Wagner-Kuhr, S. Wayand, T. Weiler, M. Zeise

Institute of Nuclear and Particle Physics (INPP), NCSR Demokritos, Aghia Paraskevi, Greece
G. Anagnostou, G. Daskalakis, T. Geralis, S. Kesisoglou, A. Kyriakis, D. Loukas, A. Markou, C. Markou, E. Ntomari, I. Topsis-giotis

University of Athens, Athens, Greece
L. Gouskos, A. Panagiotou, N. Saoulidou, E. Stiliaris

University of Ioánnina, Ioánnina, Greece
X. Aslanoglou, I. Evangelou, G. Flouris, C. Foudas, P. Kokkas, N. Manthos, I. Papadopoulos, E. Paradas

KFKI Research Institute for Particle and Nuclear Physics, Budapest, Hungary
G. Bencze, C. Hajdu, P. Hidas, D. Horvath[20], F. Sikler, V. Veszpremi, G. Vesztergombi[21], A.J. Zsigmond

Institute of Nuclear Research ATOMKI, Debrecen, Hungary
N. Beni, S. Czellar, J. Molnar, J. Palinkas, Z. Szillasi

University of Debrecen, Debrecen, Hungary
J. Karancsi, P. Raics, Z.L. Trocsanyi, B. Ujvari

National Institute of Science Education and Research, Bhubaneswar, India
S.K. Swain[22]

Panjab University, Chandigarh, India
S.B. Beri, V. Bhatnagar, N. Dhingra, R. Gupta, M. Kaur, M.Z. Mehta, M. Mittal, N. Nishu, A. Sharma, J.B. Singh

University of Delhi, Delhi, India
Ashok Kumar, Arun Kumar, S. Ahuja, A. Bhardwaj, B.C. Choudhary, S. Malhotra, M. Naimuddin, K. Ranjan, P. Saxena, V. Sharma, R.K. Shivpuri

Saha Institute of Nuclear Physics, Kolkata, India
S. Banerjee, S. Bhattacharya, K. Chatterjee, S. Dutta, B. Gomber, Sa. Jain, Sh. Jain, R. Khurana, A. Modak, S. Mukherjee, D. Roy, S. Sarkar, M. Sharan, A.P. Singh

Bhabha Atomic Research Centre, Mumbai, India
A. Abdulsalam, D. Dutta, S. Kailas, V. Kumar, A.K. Mohanty[2], L.M. Pant, P. Shukla, A. Topkar

Tata Institute of Fundamental Research - EHEP, Mumbai, India
T. Aziz, R.M. Chatterjee, S. Ganguly, S. Ghosh, M. Guchait[23], A. Gurtu[24], G. Kole, S. Kumar, M. Maity[25], G. Majumder, K. Mazumdar, G.B. Mohanty, B. Parida, K. Sudhakar, N. Wickramage[26]

Tata Institute of Fundamental Research - HECR, Mumbai, India
S. Banerjee, S. Dugad

Institute for Research in Fundamental Sciences (IPM), Tehran, Iran
H. Arfaei, H. Bakhshiansohi, S.M. Etesami[27], A. Fahim[28], A. Jafari, M. Khakzad, M. Mohammadi Najafabadi, S. Paktinat Mehdiabadi, B. Safarzadeh[29], M. Zeinali

University College Dublin, Dublin, Ireland
M. Grunewald

INFN Sezione di Bari [a], Università di Bari [b], Politecnico di Bari [c], Bari, Italy
M. Abbrescia[a,b], L. Barbone[a,b], C. Calabria[a,b], S.S. Chhibra[a,b], A. Colaleo[a], D. Creanza[a,c], N. De Filippis[a,c], M. De Palma[a,b], L. Fiore[a], G. Iaselli[a,c], G. Maggi[a,c], M. Maggi[a], B. Marangelli[a,b], S. My[a,c], S. Nuzzo[a,b], N. Pacifico[a], A. Pompili[a,b], G. Pugliese[a,c], G. Selvaggi[a,b], L. Silvestris[a], G. Singh[a,b], R. Venditti[a,b], P. Verwilligen[a], G. Zito[a]

INFN Sezione di Bologna [a], Università di Bologna [b], Bologna, Italy
G. Abbiendi[a], A.C. Benvenuti[a], D. Bonacorsi[a,b], S. Braibant-Giacomelli[a,b], L. Brigliadori[a,b], R. Campanini[a,b], P. Capiluppi[a,b], A. Castro[a,b], F.R. Cavallo[a], G. Codispoti[a,b], M. Cuffiani[a,b], G.M. Dallavalle[a], F. Fabbri[a], A. Fanfani[a,b], D. Fasanella[a,b], P. Giacomelli[a], C. Grandi[a], L. Guiducci[a,b], S. Marcellini[a], G. Masetti[a], M. Meneghelli[a,b], A. Montanari[a], F.L. Navarria[a,b], F. Odorici[a], A. Perrotta[a], F. Primavera[a,b], A.M. Rossi[a,b], T. Rovelli[a,b], G.P. Siroli[a,b], N. Tosi[a,b], R. Travaglini[a,b]

INFN Sezione di Catania [a], Università di Catania [b], Catania, Italy
S. Albergo[a,b], M. Chiorboli[a,b], S. Costa[a,b], F. Giordano[a,2], R. Potenza[a,b], A. Tricomi[a,b], C. Tuve[a,b]

INFN Sezione di Firenze [a], Università di Firenze [b], Firenze, Italy
G. Barbagli[a], V. Ciulli[a,b], C. Civinini[a], R. D'Alessandro[a,b], E. Focardi[a,b], S. Frosali[a,b], E. Gallo[a], S. Gonzi[a,b], V. Gori[a,b], P. Lenzi[a,b], M. Meschini[a], S. Paoletti[a], G. Sguazzoni[a], A. Tropiano[a,b]

INFN Laboratori Nazionali di Frascati, Frascati, Italy
L. Benussi, S. Bianco, F. Fabbri, D. Piccolo

INFN Sezione di Genova [a], Università di Genova [b], Genova, Italy
P. Fabbricatore[a], R. Ferretti[a,b], F. Ferro[a], M. Lo Vetere[a,b], R. Musenich[a], E. Robutti[a], S. Tosi[a,b]

INFN Sezione di Milano-Bicocca [a], Università di Milano-Bicocca [b], Milano, Italy
A. Benaglia[a], M.E. Dinardo[a,b], S. Fiorendi[a,b], S. Gennai[a], A. Ghezzi[a,b], P. Govoni[a,b], M.T. Lucchini[a,b,2], S. Malvezzi[a], R.A. Manzoni[a,b,2], A. Martelli[a,b,2], D. Menasce[a], L. Moroni[a], M. Paganoni[a,b], D. Pedrini[a], S. Ragazzi[a,b], N. Redaelli[a], T. Tabarelli de Fatis[a,b]

INFN Sezione di Napoli [a], Università di Napoli 'Federico II' [b], Università della Basilicata (Potenza) [c], Università G. Marconi (Roma) [d], Napoli, Italy
S. Buontempo[a], N. Cavallo[a,c], A. De Cosa[a,b], F. Fabozzi[a,c], A.O.M. Iorio[a,b], L. Lista[a], S. Meola[a,d,2], M. Merola[a], P. Paolucci[a,2]

INFN Sezione di Padova [a], Università di Padova [b], Università di Trento (Trento) [c], Padova, Italy
P. Azzi[a], N. Bacchetta[a], M. Bellato[a], D. Bisello[a,b], A. Branca[a,b], R. Carlin[a,b], P. Checchia[a],

T. Dorigo[a], U. Dosselli[a], F. Fanzago[a], M. Galanti[a,b,2], F. Gasparini[a,b], U. Gasparini[a,b], P. Giubilato[a,b], A. Gozzelino[a], K. Kanishchev[a,c], S. Lacaprara[a], I. Lazzizzera[a,c], M. Margoni[a,b], A.T. Meneguzzo[a,b], J. Pazzini[a,b], M. Pegoraro[a], N. Pozzobon[a,b], P. Ronchese[a,b], F. Simonetto[a,b], E. Torassa[a], M. Tosi[a,b], A. Triossi[a], P. Zotto[a,b], A. Zucchetta[a,b], G. Zumerle[a,b]

INFN Sezione di Pavia [a], Università di Pavia [b], Pavia, Italy
M. Gabusi[a,b], S.P. Ratti[a,b], C. Riccardi[a,b], P. Vitulo[a,b]

INFN Sezione di Perugia [a], Università di Perugia [b], Perugia, Italy
M. Biasini[a,b], G.M. Bilei[a], L. Fanò[a,b], P. Lariccia[a,b], G. Mantovani[a,b], M. Menichelli[a], A. Nappi[a,b†], F. Romeo[a,b], A. Saha[a], A. Santocchia[a,b], A. Spiezia[a,b]

INFN Sezione di Pisa [a], Università di Pisa [b], Scuola Normale Superiore di Pisa [c], Pisa, Italy
K. Androsov[a,30], P. Azzurri[a], G. Bagliesi[a], T. Boccali[a], G. Broccolo[a,c], R. Castaldi[a], M.A. Ciocci[a], R.T. D'Agnolo[a,c,2], R. Dell'Orso[a], F. Fiori[a,c], L. Foà[a,c], A. Giassi[a], M.T. Grippo[a,30], A. Kraan[a], F. Ligabue[a,c], T. Lomtadze[a], L. Martini[a,30], A. Messineo[a,b], C.S. Moon[a], F. Palla[a], A. Rizzi[a,b], A. Savoy-Navarro[a,31], A.T. Serban[a], P. Spagnolo[a], P. Squillacioti[a], R. Tenchini[a], G. Tonelli[a,b], A. Venturi[a], P.G. Verdini[a], C. Vernieri[a,c]

INFN Sezione di Roma [a], Università di Roma [b], Roma, Italy
L. Barone[a,b], F. Cavallari[a], D. Del Re[a,b], M. Diemoz[a], M. Grassi[a,b], E. Longo[a,b], F. Margaroli[a,b], P. Meridiani[a], F. Micheli[a,b], S. Nourbakhsh[a,b], G. Organtini[a,b], R. Paramatti[a], S. Rahatlou[a,b], C. Rovelli[a], L. Soffi[a,b]

INFN Sezione di Torino [a], Università di Torino [b], Università del Piemonte Orientale (Novara) [c], Torino, Italy
N. Amapane[a,b], R. Arcidiacono[a,c], S. Argiro[a,b], M. Arneodo[a,c], R. Bellan[a,b], C. Biino[a], N. Cartiglia[a], S. Casasso[a,b], M. Costa[a,b], A. Degano[a,b], N. Demaria[a], C. Mariotti[a], S. Maselli[a], E. Migliore[a,b], V. Monaco[a,b], M. Musich[a], M.M. Obertino[a,c], N. Pastrone[a], M. Pelliccioni[a,2], A. Potenza[a,b], A. Romero[a,b], M. Ruspa[a,c], R. Sacchi[a,b], A. Solano[a,b], A. Staiano[a], U. Tamponi[a]

INFN Sezione di Trieste [a], Università di Trieste [b], Trieste, Italy
S. Belforte[a], V. Candelise[a,b], M. Casarsa[a], F. Cossutti[a,2], G. Della Ricca[a,b], B. Gobbo[a], C. La Licata[a,b], M. Marone[a,b], D. Montanino[a,b], A. Penzo[a], A. Schizzi[a,b], A. Zanetti[a]

Kangwon National University, Chunchon, Korea
S. Chang, T.Y. Kim, S.K. Nam

Kyungpook National University, Daegu, Korea
D.H. Kim, G.N. Kim, J.E. Kim, D.J. Kong, S. Lee, Y.D. Oh, H. Park, D.C. Son

Chonnam National University, Institute for Universe and Elementary Particles, Kwangju, Korea
J.Y. Kim, Zero J. Kim, S. Song

Korea University, Seoul, Korea
S. Choi, D. Gyun, B. Hong, M. Jo, H. Kim, T.J. Kim, K.S. Lee, S.K. Park, Y. Roh

University of Seoul, Seoul, Korea
M. Choi, J.H. Kim, C. Park, I.C. Park, S. Park, G. Ryu

Sungkyunkwan University, Suwon, Korea
Y. Choi, Y.K. Choi, J. Goh, M.S. Kim, E. Kwon, B. Lee, J. Lee, S. Lee, H. Seo, I. Yu

Vilnius University, Vilnius, Lithuania
I. Grigelionis, A. Juodagalvis

Centro de Investigacion y de Estudios Avanzados del IPN, Mexico City, Mexico
H. Castilla-Valdez, E. De La Cruz-Burelo, I. Heredia-de La Cruz[32], R. Lopez-Fernandez, J. Martínez-Ortega, A. Sanchez-Hernandez, L.M. Villasenor-Cendejas

Universidad Iberoamericana, Mexico City, Mexico
S. Carrillo Moreno, F. Vazquez Valencia

Benemerita Universidad Autonoma de Puebla, Puebla, Mexico
H.A. Salazar Ibarguen

Universidad Autónoma de San Luis Potosí, San Luis Potosí, Mexico
E. Casimiro Linares, A. Morelos Pineda, M.A. Reyes-Santos

University of Auckland, Auckland, New Zealand
D. Krofcheck

University of Canterbury, Christchurch, New Zealand
P.H. Butler, R. Doesburg, S. Reucroft, H. Silverwood

National Centre for Physics, Quaid-I-Azam University, Islamabad, Pakistan
M. Ahmad, M.I. Asghar, J. Butt, H.R. Hoorani, S. Khalid, W.A. Khan, T. Khurshid, S. Qazi, M.A. Shah, M. Shoaib

National Centre for Nuclear Research, Swierk, Poland
H. Bialkowska, B. Boimska, T. Frueboes, M. Górski, M. Kazana, K. Nawrocki, K. Romanowska-Rybinska, M. Szleper, G. Wrochna, P. Zalewski

Institute of Experimental Physics, Faculty of Physics, University of Warsaw, Warsaw, Poland
G. Brona, K. Bunkowski, M. Cwiok, W. Dominik, K. Doroba, A. Kalinowski, M. Konecki, J. Krolikowski, M. Misiura, W. Wolszczak

Laboratório de Instrumentação e Física Experimental de Partículas, Lisboa, Portugal
N. Almeida, P. Bargassa, C. Beirão Da Cruz E Silva, P. Faccioli, P.G. Ferreira Parracho, M. Gallinaro, F. Nguyen, J. Rodrigues Antunes, J. Seixas[2], J. Varela, P. Vischia

Joint Institute for Nuclear Research, Dubna, Russia
S. Afanasiev, P. Bunin, M. Gavrilenko, I. Golutvin, I. Gorbunov, A. Kamenev, V. Karjavin, V. Konoplyanikov, A. Lanev, A. Malakhov, V. Matveev, P. Moisenz, V. Palichik, V. Perelygin, S. Shmatov, N. Skatchkov, V. Smirnov, A. Zarubin

Petersburg Nuclear Physics Institute, Gatchina (St. Petersburg), Russia
S. Evstyukhin, V. Golovtsov, Y. Ivanov, V. Kim, P. Levchenko, V. Murzin, V. Oreshkin, I. Smirnov, V. Sulimov, L. Uvarov, S. Vavilov, A. Vorobyev, An. Vorobyev

Institute for Nuclear Research, Moscow, Russia
Yu. Andreev, A. Dermenev, S. Gninenko, N. Golubev, M. Kirsanov, N. Krasnikov, A. Pashenkov, D. Tlisov, A. Toropin

Institute for Theoretical and Experimental Physics, Moscow, Russia
V. Epshteyn, M. Erofeeva, V. Gavrilov, N. Lychkovskaya, V. Popov, G. Safronov, S. Semenov, A. Spiridonov, V. Stolin, E. Vlasov, A. Zhokin

P.N. Lebedev Physical Institute, Moscow, Russia
V. Andreev, M. Azarkin, I. Dremin, M. Kirakosyan, A. Leonidov, G. Mesyats, S.V. Rusakov, A. Vinogradov

Skobeltsyn Institute of Nuclear Physics, Lomonosov Moscow State University, Moscow, Russia
A. Belyaev, E. Boos, V. Bunichev, M. Dubinin[7], L. Dudko, A. Gribushin, V. Klyukhin, O. Kodolova, I. Lokhtin, A. Markina, S. Obraztsov, M. Perfilov, V. Savrin, N. Tsirova

State Research Center of Russian Federation, Institute for High Energy Physics, Protvino, Russia
I. Azhgirey, I. Bayshev, S. Bitioukov, V. Kachanov, A. Kalinin, D. Konstantinov, V. Krychkine, V. Petrov, R. Ryutin, A. Sobol, L. Tourtchanovitch, S. Troshin, N. Tyurin, A. Uzunian, A. Volkov

University of Belgrade, Faculty of Physics and Vinca Institute of Nuclear Sciences, Belgrade, Serbia
P. Adzic[33], M. Djordjevic, M. Ekmedzic, D. Krpic[33], J. Milosevic

Centro de Investigaciones Energéticas Medioambientales y Tecnológicas (CIEMAT), Madrid, Spain
M. Aguilar-Benitez, J. Alcaraz Maestre, C. Battilana, E. Calvo, M. Cerrada, M. Chamizo Llatas[2], N. Colino, B. De La Cruz, A. Delgado Peris, D. Domínguez Vázquez, C. Fernandez Bedoya, J.P. Fernández Ramos, A. Ferrando, J. Flix, M.C. Fouz, P. Garcia-Abia, O. Gonzalez Lopez, S. Goy Lopez, J.M. Hernandez, M.I. Josa, G. Merino, E. Navarro De Martino, J. Puerta Pelayo, A. Quintario Olmeda, I. Redondo, L. Romero, J. Santaolalla, M.S. Soares, C. Willmott

Universidad Autónoma de Madrid, Madrid, Spain
C. Albajar, J.F. de Trocóniz

Universidad de Oviedo, Oviedo, Spain
H. Brun, J. Cuevas, J. Fernandez Menendez, S. Folgueras, I. Gonzalez Caballero, L. Lloret Iglesias, J. Piedra Gomez

Instituto de Física de Cantabria (IFCA), CSIC-Universidad de Cantabria, Santander, Spain
J.A. Brochero Cifuentes, I.J. Cabrillo, A. Calderon, S.H. Chuang, J. Duarte Campderros, M. Fernandez, G. Gomez, J. Gonzalez Sanchez, A. Graziano, C. Jorda, A. Lopez Virto, J. Marco, R. Marco, C. Martinez Rivero, F. Matorras, F.J. Munoz Sanchez, T. Rodrigo, A.Y. Rodríguez-Marrero, A. Ruiz-Jimeno, L. Scodellaro, I. Vila, R. Vilar Cortabitarte

CERN, European Organization for Nuclear Research, Geneva, Switzerland
D. Abbaneo, E. Auffray, G. Auzinger, M. Bachtis, P. Baillon, A.H. Ball, D. Barney, J. Bendavid, J.F. Benitez, C. Bernet[8], G. Bianchi, P. Bloch, A. Bocci, A. Bonato, O. Bondu, C. Botta, H. Breuker, T. Camporesi, G. Cerminara, T. Christiansen, J.A. Coarasa Perez, S. Colafranceschi[34], M. D'Alfonso, D. d'Enterria, A. Dabrowski, A. David, F. De Guio, A. De Roeck, S. De Visscher, S. Di Guida, M. Dobson, N. Dupont-Sagorin, A. Elliott-Peisert, J. Eugster, W. Funk, G. Georgiou, M. Giffels, D. Gigi, K. Gill, D. Giordano, M. Girone, M. Giunta, F. Glege, R. Gomez-Reino Garrido, S. Gowdy, R. Guida, J. Hammer, M. Hansen, P. Harris, C. Hartl, A. Hinzmann, V. Innocente, P. Janot, E. Karavakis, K. Kousouris, K. Krajczar, P. Lecoq, Y.-J. Lee, C. Lourenço, N. Magini, L. Malgeri, M. Mannelli, L. Masetti, F. Meijers, S. Mersi, E. Meschi, R. Moser, M. Mulders, P. Musella, E. Nesvold, L. Orsini, E. Palencia Cortezon, E. Perez, L. Perrozzi, A. Petrilli, A. Pfeiffer, M. Pierini, M. Pimiä, D. Piparo, M. Plagge, L. Quertenmont, A. Racz, W. Reece, G. Rolandi[35], M. Rovere, H. Sakulin, F. Santanastasio, C. Schäfer, C. Schwick, I. Segoni, S. Sekmen, A. Sharma, P. Siegrist, P. Silva, M. Simon, P. Sphicas[36], D. Spiga, M. Stoye, A. Tsirou, G.I. Veres[21], J.R. Vlimant, H.K. Wöhri, S.D. Worm[37], W.D. Zeuner

Paul Scherrer Institut, Villigen, Switzerland

W. Bertl, K. Deiters, W. Erdmann, K. Gabathuler, R. Horisberger, Q. Ingram, H.C. Kaestli, S. König, D. Kotlinski, U. Langenegger, D. Renker, T. Rohe

Institute for Particle Physics, ETH Zurich, Zurich, Switzerland
F. Bachmair, L. Bäni, L. Bianchini, P. Bortignon, M.A. Buchmann, B. Casal, N. Chanon, A. Deisher, G. Dissertori, M. Dittmar, M. Donegà, M. Dünser, P. Eller, K. Freudenreich, C. Grab, D. Hits, P. Lecomte, W. Lustermann, B. Mangano, A.C. Marini, P. Martinez Ruiz del Arbol, D. Meister, N. Mohr, F. Moortgat, C. Nägeli[38], P. Nef, F. Nessi-Tedaldi, F. Pandolfi, L. Pape, F. Pauss, M. Peruzzi, F.J. Ronga, M. Rossini, L. Sala, A.K. Sanchez, A. Starodumov[39], B. Stieger, M. Takahashi, L. Tauscher[†], A. Thea, K. Theofilatos, D. Treille, C. Urscheler, R. Wallny, H.A. Weber

Universität Zürich, Zurich, Switzerland
C. Amsler[40], V. Chiochia, C. Favaro, M. Ivova Rikova, B. Kilminster, B. Millan Mejias, P. Robmann, H. Snoek, S. Taroni, M. Verzetti, Y. Yang

National Central University, Chung-Li, Taiwan
M. Cardaci, K.H. Chen, C. Ferro, C.M. Kuo, S.W. Li, W. Lin, Y.J. Lu, R. Volpe, S.S. Yu

National Taiwan University (NTU), Taipei, Taiwan
P. Bartalini, P. Chang, Y.H. Chang, Y.W. Chang, Y. Chao, K.F. Chen, C. Dietz, U. Grundler, W.-S. Hou, Y. Hsiung, K.Y. Kao, Y.J. Lei, R.-S. Lu, D. Majumder, E. Petrakou, X. Shi, J.G. Shiu, Y.M. Tzeng, M. Wang

Chulalongkorn University, Bangkok, Thailand
B. Asavapibhop, N. Suwonjandee

Cukurova University, Adana, Turkey
A. Adiguzel, M.N. Bakirci[41], S. Cerci[42], C. Dozen, I. Dumanoglu, E. Eskut, S. Girgis, G. Gokbulut, E. Gurpinar, I. Hos, E.E. Kangal, A. Kayis Topaksu, G. Onengut[43], K. Ozdemir, S. Ozturk[41], A. Polatoz, K. Sogut[44], D. Sunar Cerci[42], B. Tali[42], H. Topakli[41], M. Vergili

Middle East Technical University, Physics Department, Ankara, Turkey
I.V. Akin, T. Aliev, B. Bilin, S. Bilmis, M. Deniz, H. Gamsizkan, A.M. Guler, G. Karapinar[45], K. Ocalan, A. Ozpineci, M. Serin, R. Sever, U.E. Surat, M. Yalvac, M. Zeyrek

Bogazici University, Istanbul, Turkey
E. Gülmez, B. Isildak[46], M. Kaya[47], O. Kaya[47], S. Ozkorucuklu[48], N. Sonmez[49]

Istanbul Technical University, Istanbul, Turkey
H. Bahtiyar[50], E. Barlas, K. Cankocak, Y.O. Günaydin[51], F.I. Vardarlı, M. Yücel

National Scientific Center, Kharkov Institute of Physics and Technology, Kharkov, Ukraine
L. Levchuk, P. Sorokin

University of Bristol, Bristol, United Kingdom
J.J. Brooke, E. Clement, D. Cussans, H. Flacher, R. Frazier, J. Goldstein, M. Grimes, G.P. Heath, H.F. Heath, L. Kreczko, C. Lucas, Z. Meng, S. Metson, D.M. Newbold[37], K. Nirunpong, S. Paramesvaran, A. Poll, S. Senkin, V.J. Smith, T. Williams

Rutherford Appleton Laboratory, Didcot, United Kingdom
K.W. Bell, A. Belyaev[52], C. Brew, R.M. Brown, D.J.A. Cockerill, J.A. Coughlan, K. Harder, S. Harper, E. Olaiya, D. Petyt, B.C. Radburn-Smith, C.H. Shepherd-Themistocleous, I.R. Tomalin, W.J. Womersley

Imperial College, London, United Kingdom
R. Bainbridge, O. Buchmuller, D. Burton, D. Colling, N. Cripps, M. Cutajar, P. Dauncey, G. Davies, M. Della Negra, W. Ferguson, J. Fulcher, D. Futyan, A. Gilbert, A. Guneratne Bryer, G. Hall, Z. Hatherell, J. Hays, G. Iles, M. Jarvis, G. Karapostoli, M. Kenzie, R. Lane, R. Lucas[37], L. Lyons, A.-M. Magnan, J. Marrouche, B. Mathias, R. Nandi, J. Nash, A. Nikitenko[39], J. Pela, M. Pesaresi, K. Petridis, M. Pioppi[53], D.M. Raymond, S. Rogerson, A. Rose, C. Seez, P. Sharp†, A. Sparrow, A. Tapper, M. Vazquez Acosta, T. Virdee, S. Wakefield, N. Wardle

Brunel University, Uxbridge, United Kingdom
M. Chadwick, J.E. Cole, P.R. Hobson, A. Khan, P. Kyberd, D. Leggat, D. Leslie, W. Martin, I.D. Reid, P. Symonds, L. Teodorescu, M. Turner

Baylor University, Waco, USA
J. Dittmann, K. Hatakeyama, A. Kasmi, H. Liu, T. Scarborough

The University of Alabama, Tuscaloosa, USA
O. Charaf, S.I. Cooper, C. Henderson, P. Rumerio

Boston University, Boston, USA
A. Avetisyan, T. Bose, C. Fantasia, A. Heister, P. Lawson, D. Lazic, J. Rohlf, D. Sperka, J. St. John, L. Sulak

Brown University, Providence, USA
J. Alimena, S. Bhattacharya, G. Christopher, D. Cutts, Z. Demiragli, A. Ferapontov, A. Garabedian, U. Heintz, S. Jabeen, G. Kukartsev, E. Laird, G. Landsberg, M. Luk, M. Narain, M. Segala, T. Sinthuprasith, T. Speer

University of California, Davis, Davis, USA
R. Breedon, G. Breto, M. Calderon De La Barca Sanchez, S. Chauhan, M. Chertok, J. Conway, R. Conway, P.T. Cox, R. Erbacher, M. Gardner, R. Houtz, W. Ko, A. Kopecky, R. Lander, T. Miceli, D. Pellett, J. Pilot, F. Ricci-Tam, B. Rutherford, M. Searle, J. Smith, M. Squires, M. Tripathi, S. Wilbur, R. Yohay

University of California, Los Angeles, USA
V. Andreev, D. Cline, R. Cousins, S. Erhan, P. Everaerts, C. Farrell, M. Felcini, J. Hauser, M. Ignatenko, C. Jarvis, G. Rakness, P. Schlein†, E. Takasugi, P. Traczyk, V. Valuev, M. Weber

University of California, Riverside, Riverside, USA
J. Babb, R. Clare, J. Ellison, J.W. Gary, G. Hanson, J. Heilman, P. Jandir, H. Liu, O.R. Long, A. Luthra, M. Malberti, H. Nguyen, A. Shrinivas, J. Sturdy, S. Sumowidagdo, R. Wilken, S. Wimpenny

University of California, San Diego, La Jolla, USA
W. Andrews, J.G. Branson, G.B. Cerati, S. Cittolin, D. Evans, A. Holzner, R. Kelley, M. Lebourgeois, J. Letts, I. Macneill, S. Padhi, C. Palmer, G. Petrucciani, M. Pieri, M. Sani, V. Sharma, S. Simon, E. Sudano, M. Tadel, Y. Tu, A. Vartak, S. Wasserbaech[54], F. Würthwein, A. Yagil, J. Yoo

University of California, Santa Barbara, Santa Barbara, USA
D. Barge, C. Campagnari, T. Danielson, K. Flowers, P. Geffert, C. George, F. Golf, J. Incandela, C. Justus, D. Kovalskyi, V. Krutelyov, S. Lowette, R. Magaña Villalba, N. Mccoll, V. Pavlunin, J. Richman, R. Rossin, D. Stuart, W. To, C. West

California Institute of Technology, Pasadena, USA
A. Apresyan, A. Bornheim, J. Bunn, Y. Chen, E. Di Marco, J. Duarte, D. Kcira, Y. Ma, A. Mott,

H.B. Newman, C. Pena, C. Rogan, M. Spiropulu, V. Timciuc, J. Veverka, R. Wilkinson, S. Xie, R.Y. Zhu

Carnegie Mellon University, Pittsburgh, USA
V. Azzolini, A. Calamba, R. Carroll, T. Ferguson, Y. Iiyama, D.W. Jang, Y.F. Liu, M. Paulini, J. Russ, H. Vogel, I. Vorobiev

University of Colorado at Boulder, Boulder, USA
J.P. Cumalat, B.R. Drell, W.T. Ford, A. Gaz, E. Luiggi Lopez, U. Nauenberg, J.G. Smith, K. Stenson, K.A. Ulmer, S.R. Wagner

Cornell University, Ithaca, USA
J. Alexander, A. Chatterjee, N. Eggert, L.K. Gibbons, W. Hopkins, A. Khukhunaishvili, B. Kreis, N. Mirman, G. Nicolas Kaufman, J.R. Patterson, A. Ryd, E. Salvati, W. Sun, W.D. Teo, J. Thom, J. Thompson, J. Tucker, Y. Weng, L. Winstrom, P. Wittich

Fairfield University, Fairfield, USA
D. Winn

Fermi National Accelerator Laboratory, Batavia, USA
S. Abdullin, M. Albrow, J. Anderson, G. Apollinari, L.A.T. Bauerdick, A. Beretvas, J. Berryhill, P.C. Bhat, K. Burkett, J.N. Butler, V. Chetluru, H.W.K. Cheung, F. Chlebana, S. Cihangir, V.D. Elvira, I. Fisk, J. Freeman, Y. Gao, E. Gottschalk, L. Gray, D. Green, O. Gutsche, D. Hare, R.M. Harris, J. Hirschauer, B. Hooberman, S. Jindariani, M. Johnson, U. Joshi, K. Kaadze, B. Klima, S. Kunori, S. Kwan, J. Linacre, D. Lincoln, R. Lipton, J. Lykken, K. Maeshima, J.M. Marraffino, V.I. Martinez Outschoorn, S. Maruyama, D. Mason, P. McBride, K. Mishra, S. Mrenna, Y. Musienko[55], C. Newman-Holmes, V. O'Dell, O. Prokofyev, N. Ratnikova, E. Sexton-Kennedy, S. Sharma, W.J. Spalding, L. Spiegel, L. Taylor, S. Tkaczyk, N.V. Tran, L. Uplegger, E.W. Vaandering, R. Vidal, J. Whitmore, W. Wu, F. Yang, J.C. Yun

University of Florida, Gainesville, USA
D. Acosta, P. Avery, D. Bourilkov, M. Chen, T. Cheng, S. Das, M. De Gruttola, G.P. Di Giovanni, D. Dobur, A. Drozdetskiy, R.D. Field, M. Fisher, Y. Fu, I.K. Furic, J. Hugon, B. Kim, J. Konigsberg, A. Korytov, A. Kropivnitskaya, T. Kypreos, J.F. Low, K. Matchev, P. Milenovic[56], G. Mitselmakher, L. Muniz, R. Remington, A. Rinkevicius, N. Skhirtladze, M. Snowball, J. Yelton, M. Zakaria

Florida International University, Miami, USA
V. Gaultney, S. Hewamanage, S. Linn, P. Markowitz, G. Martinez, J.L. Rodriguez

Florida State University, Tallahassee, USA
T. Adams, A. Askew, J. Bochenek, J. Chen, B. Diamond, S.V. Gleyzer, J. Haas, S. Hagopian, V. Hagopian, K.F. Johnson, H. Prosper, V. Veeraraghavan, M. Weinberg

Florida Institute of Technology, Melbourne, USA
M.M. Baarmand, B. Dorney, M. Hohlmann, H. Kalakhety, F. Yumiceva

University of Illinois at Chicago (UIC), Chicago, USA
M.R. Adams, L. Apanasevich, V.E. Bazterra, R.R. Betts, I. Bucinskaite, J. Callner, R. Cavanaugh, O. Evdokimov, L. Gauthier, C.E. Gerber, D.J. Hofman, S. Khalatyan, P. Kurt, F. Lacroix, D.H. Moon, C. O'Brien, C. Silkworth, D. Strom, P. Turner, N. Varelas

The University of Iowa, Iowa City, USA
U. Akgun, E.A. Albayrak[50], B. Bilki[57], W. Clarida, K. Dilsiz, F. Duru, S. Griffiths, J.-P. Merlo,

H. Mermerkaya[58], A. Mestvirishvili, A. Moeller, J. Nachtman, C.R. Newsom, H. Ogul, Y. Onel, F. Ozok[50], S. Sen, P. Tan, E. Tiras, J. Wetzel, T. Yetkin[59], K. Yi

Johns Hopkins University, Baltimore, USA
B.A. Barnett, B. Blumenfeld, S. Bolognesi, G. Giurgiu, A.V. Gritsan, G. Hu, P. Maksimovic, C. Martin, M. Swartz, A. Whitbeck

The University of Kansas, Lawrence, USA
P. Baringer, A. Bean, G. Benelli, R.P. Kenny III, M. Murray, D. Noonan, S. Sanders, R. Stringer, J.S. Wood

Kansas State University, Manhattan, USA
A.F. Barfuss, I. Chakaberia, A. Ivanov, S. Khalil, M. Makouski, Y. Maravin, L.K. Saini, S. Shrestha, I. Svintradze

Lawrence Livermore National Laboratory, Livermore, USA
J. Gronberg, D. Lange, F. Rebassoo, D. Wright

University of Maryland, College Park, USA
A. Baden, B. Calvert, S.C. Eno, J.A. Gomez, N.J. Hadley, R.G. Kellogg, T. Kolberg, Y. Lu, M. Marionneau, A.C. Mignerey, K. Pedro, A. Peterman, A. Skuja, J. Temple, M.B. Tonjes, S.C. Tonwar

Massachusetts Institute of Technology, Cambridge, USA
A. Apyan, G. Bauer, W. Busza, I.A. Cali, M. Chan, L. Di Matteo, V. Dutta, G. Gomez Ceballos, M. Goncharov, D. Gulhan, Y. Kim, M. Klute, Y.S. Lai, A. Levin, P.D. Luckey, T. Ma, S. Nahn, C. Paus, D. Ralph, C. Roland, G. Roland, G.S.F. Stephans, F. Stöckli, K. Sumorok, D. Velicanu, R. Wolf, B. Wyslouch, M. Yang, Y. Yilmaz, A.S. Yoon, M. Zanetti, V. Zhukova

University of Minnesota, Minneapolis, USA
B. Dahmes, A. De Benedetti, G. Franzoni, A. Gude, J. Haupt, S.C. Kao, K. Klapoetke, Y. Kubota, J. Mans, N. Pastika, R. Rusack, M. Sasseville, A. Singovsky, N. Tambe, J. Turkewitz

University of Mississippi, Oxford, USA
J.G. Acosta, L.M. Cremaldi, R. Kroeger, S. Oliveros, L. Perera, R. Rahmat, D.A. Sanders, D. Summers

University of Nebraska-Lincoln, Lincoln, USA
E. Avdeeva, K. Bloom, S. Bose, D.R. Claes, A. Dominguez, M. Eads, R. Gonzalez Suarez, J. Keller, I. Kravchenko, J. Lazo-Flores, S. Malik, F. Meier, G.R. Snow

State University of New York at Buffalo, Buffalo, USA
J. Dolen, A. Godshalk, I. Iashvili, S. Jain, A. Kharchilava, A. Kumar, S. Rappoccio, Z. Wan

Northeastern University, Boston, USA
G. Alverson, E. Barberis, D. Baumgartel, M. Chasco, J. Haley, A. Massironi, D. Nash, T. Orimoto, D. Trocino, D. Wood, J. Zhang

Northwestern University, Evanston, USA
A. Anastassov, K.A. Hahn, A. Kubik, L. Lusito, N. Mucia, N. Odell, B. Pollack, A. Pozdnyakov, M. Schmitt, S. Stoynev, K. Sung, M. Velasco, S. Won

University of Notre Dame, Notre Dame, USA
D. Berry, A. Brinkerhoff, K.M. Chan, M. Hildreth, C. Jessop, D.J. Karmgard, J. Kolb, K. Lannon, W. Luo, S. Lynch, N. Marinelli, D.M. Morse, T. Pearson, M. Planer, R. Ruchti, J. Slaunwhite, N. Valls, M. Wayne, M. Wolf

The Ohio State University, Columbus, USA
L. Antonelli, B. Bylsma, L.S. Durkin, C. Hill, R. Hughes, K. Kotov, T.Y. Ling, D. Puigh, M. Rodenburg, G. Smith, C. Vuosalo, B.L. Winer, H. Wolfe

Princeton University, Princeton, USA
E. Berry, P. Elmer, V. Halyo, P. Hebda, J. Hegeman, A. Hunt, P. Jindal, S.A. Koay, P. Lujan, D. Marlow, T. Medvedeva, M. Mooney, J. Olsen, P. Piroué, X. Quan, A. Raval, H. Saka, D. Stickland, C. Tully, J.S. Werner, S.C. Zenz, A. Zuranski

University of Puerto Rico, Mayaguez, USA
E. Brownson, A. Lopez, H. Mendez, J.E. Ramirez Vargas

Purdue University, West Lafayette, USA
E. Alagoz, D. Benedetti, G. Bolla, D. Bortoletto, M. De Mattia, A. Everett, Z. Hu, M. Jones, K. Jung, O. Koybasi, M. Kress, N. Leonardo, D. Lopes Pegna, V. Maroussov, P. Merkel, D.H. Miller, N. Neumeister, I. Shipsey, D. Silvers, A. Svyatkovskiy, M. Vidal Marono, F. Wang, W. Xie, L. Xu, H.D. Yoo, J. Zablocki, Y. Zheng

Purdue University Calumet, Hammond, USA
N. Parashar

Rice University, Houston, USA
A. Adair, B. Akgun, K.M. Ecklund, F.J.M. Geurts, W. Li, B. Michlin, B.P. Padley, R. Redjimi, J. Roberts, J. Zabel

University of Rochester, Rochester, USA
B. Betchart, A. Bodek, R. Covarelli, P. de Barbaro, R. Demina, Y. Eshaq, T. Ferbel, A. Garcia-Bellido, P. Goldenzweig, J. Han, A. Harel, D.C. Miner, G. Petrillo, D. Vishnevskiy, M. Zielinski

The Rockefeller University, New York, USA
A. Bhatti, R. Ciesielski, L. Demortier, K. Goulianos, G. Lungu, S. Malik, C. Mesropian

Rutgers, The State University of New Jersey, Piscataway, USA
S. Arora, A. Barker, J.P. Chou, C. Contreras-Campana, E. Contreras-Campana, D. Duggan, D. Ferencek, Y. Gershtein, R. Gray, E. Halkiadakis, D. Hidas, A. Lath, S. Panwalkar, M. Park, R. Patel, V. Rekovic, J. Robles, S. Salur, S. Schnetzer, C. Seitz, S. Somalwar, R. Stone, S. Thomas, P. Thomassen, M. Walker

University of Tennessee, Knoxville, USA
G. Cerizza, M. Hollingsworth, K. Rose, S. Spanier, Z.C. Yang, A. York

Texas A&M University, College Station, USA
O. Bouhali[60], R. Eusebi, W. Flanagan, J. Gilmore, T. Kamon[61], V. Khotilovich, R. Montalvo, I. Osipenkov, Y. Pakhotin, A. Perloff, J. Roe, A. Safonov, T. Sakuma, I. Suarez, A. Tatarinov, D. Toback

Texas Tech University, Lubbock, USA
N. Akchurin, C. Cowden, J. Damgov, C. Dragoiu, P.R. Dudero, K. Kovitanggoon, S.W. Lee, T. Libeiro, I. Volobouev

Vanderbilt University, Nashville, USA
E. Appelt, A.G. Delannoy, S. Greene, A. Gurrola, W. Johns, C. Maguire, Y. Mao, A. Melo, M. Sharma, P. Sheldon, B. Snook, S. Tuo, J. Velkovska

University of Virginia, Charlottesville, USA
M.W. Arenton, S. Boutle, B. Cox, B. Francis, J. Goodell, R. Hirosky, A. Ledovskoy, C. Lin, C. Neu, J. Wood

Wayne State University, Detroit, USA
S. Gollapinni, R. Harr, P.E. Karchin, C. Kottachchi Kankanamge Don, P. Lamichhane, A. Sakharov

University of Wisconsin, Madison, USA
D.A. Belknap, L. Borrello, D. Carlsmith, M. Cepeda, S. Dasu, S. Duric, E. Friis, M. Grothe, R. Hall-Wilton, M. Herndon, A. Hervé, P. Klabbers, J. Klukas, A. Lanaro, R. Loveless, A. Mohapatra, M.U. Mozer, I. Ojalvo, T. Perry, G.A. Pierro, G. Polese, I. Ross, T. Sarangi, A. Savin, W.H. Smith, J. Swanson

†: Deceased
1: Also at Vienna University of Technology, Vienna, Austria
2: Also at CERN, European Organization for Nuclear Research, Geneva, Switzerland
3: Also at Institut Pluridisciplinaire Hubert Curien, Université de Strasbourg, Université de Haute Alsace Mulhouse, CNRS/IN2P3, Strasbourg, France
4: Also at National Institute of Chemical Physics and Biophysics, Tallinn, Estonia
5: Also at Skobeltsyn Institute of Nuclear Physics, Lomonosov Moscow State University, Moscow, Russia
6: Also at Universidade Estadual de Campinas, Campinas, Brazil
7: Also at California Institute of Technology, Pasadena, USA
8: Also at Laboratoire Leprince-Ringuet, Ecole Polytechnique, IN2P3-CNRS, Palaiseau, France
9: Also at Suez Canal University, Suez, Egypt
10: Also at Zewail City of Science and Technology, Zewail, Egypt
11: Also at Cairo University, Cairo, Egypt
12: Also at Fayoum University, El-Fayoum, Egypt
13: Also at British University in Egypt, Cairo, Egypt
14: Now at Ain Shams University, Cairo, Egypt
15: Also at National Centre for Nuclear Research, Swierk, Poland
16: Also at Université de Haute Alsace, Mulhouse, France
17: Also at Joint Institute for Nuclear Research, Dubna, Russia
18: Also at Brandenburg University of Technology, Cottbus, Germany
19: Also at The University of Kansas, Lawrence, USA
20: Also at Institute of Nuclear Research ATOMKI, Debrecen, Hungary
21: Also at Eötvös Loránd University, Budapest, Hungary
22: Also at Tata Institute of Fundamental Research - EHEP, Mumbai, India
23: Also at Tata Institute of Fundamental Research - HECR, Mumbai, India
24: Now at King Abdulaziz University, Jeddah, Saudi Arabia
25: Also at University of Visva-Bharati, Santiniketan, India
26: Also at University of Ruhuna, Matara, Sri Lanka
27: Also at Isfahan University of Technology, Isfahan, Iran
28: Also at Sharif University of Technology, Tehran, Iran
29: Also at Plasma Physics Research Center, Science and Research Branch, Islamic Azad University, Tehran, Iran
30: Also at Università degli Studi di Siena, Siena, Italy
31: Also at Purdue University, West Lafayette, USA
32: Also at Universidad Michoacana de San Nicolas de Hidalgo, Morelia, Mexico
33: Also at Faculty of Physics, University of Belgrade, Belgrade, Serbia

34: Also at Facoltà Ingegneria, Università di Roma, Roma, Italy
35: Also at Scuola Normale e Sezione dell'INFN, Pisa, Italy
36: Also at University of Athens, Athens, Greece
37: Also at Rutherford Appleton Laboratory, Didcot, United Kingdom
38: Also at Paul Scherrer Institut, Villigen, Switzerland
39: Also at Institute for Theoretical and Experimental Physics, Moscow, Russia
40: Also at Albert Einstein Center for Fundamental Physics, Bern, Switzerland
41: Also at Gaziosmanpasa University, Tokat, Turkey
42: Also at Adiyaman University, Adiyaman, Turkey
43: Also at Cag University, Mersin, Turkey
44: Also at Mersin University, Mersin, Turkey
45: Also at Izmir Institute of Technology, Izmir, Turkey
46: Also at Ozyegin University, Istanbul, Turkey
47: Also at Kafkas University, Kars, Turkey
48: Also at Suleyman Demirel University, Isparta, Turkey
49: Also at Ege University, Izmir, Turkey
50: Also at Mimar Sinan University, Istanbul, Istanbul, Turkey
51: Also at Kahramanmaras Sütcü Imam University, Kahramanmaras, Turkey
52: Also at School of Physics and Astronomy, University of Southampton, Southampton, United Kingdom
53: Also at INFN Sezione di Perugia; Università di Perugia, Perugia, Italy
54: Also at Utah Valley University, Orem, USA
55: Also at Institute for Nuclear Research, Moscow, Russia
56: Also at University of Belgrade, Faculty of Physics and Vinca Institute of Nuclear Sciences, Belgrade, Serbia
57: Also at Argonne National Laboratory, Argonne, USA
58: Also at Erzincan University, Erzincan, Turkey
59: Also at Yildiz Technical University, Istanbul, Turkey
60: Also at Texas A&M University at Qatar, Doha, Qatar
61: Also at Kyungpook National University, Daegu, Korea